DETERMINATION OF CAPILLARY PRESSURE, RELATIVE PERMEABILITY AND PORES SIZE DISTRIBUTION CHARACTERISTICS OF COAL FROM SYDNEY BASIN-CANADA

by

Anita Nourbakhsh

Submitted in partial fulfilment of the requirements
for the degree of Master of Applied Science

at

Dalhousie University
Halifax, Nova Scotia
August 2012

DALHOUSIE UNIVERSITY

DEPARTMENT OF PROCESS ENGINEERING AND APPLIED SCIENCE

The undersigned hereby certify that they have read and recommend to the Faculty of Graduate Studies for acceptance a thesis entitled "**DETERMINATION OF CAPILLARY PRESSURE, RELATIVE PERMEABILITY AND PORES SIZE DISTRIBUTION CHARACTERISTICS OF COAL FROM SYDNEY BASIN-CANADA**" by Anita Nourbakhsh in partial fulfilment of the requirements for the degree of Master of Applied Science.

Dated: 13 August, 2012

Supervisor: _________________________________

Readers: _________________________________

____

DALHOUSIE UNIVERSITY

DATE: 13 August 2012

AUTHOR: Anita Nourbakhsh

TITLE: DETERMINATION OF CAPILLARY PRESSURE, RELATIVE PERMEABILITY AND PORES SIZE DISTRIBUTION CHARACTERISTICS OF COAL FROM SYDNEY BASIN-CANADA

DEPARTMENT OR SCHOOL: Department Process Engineering and Applied Science

DEGREE: MASc CONVOCATION: October YEAR: 2012

____

Signature of Author

TABLE OF CONTENTS

LIST OF TABLES

LIST OF FIGURES

ABSTRACT

Global warming due to anthropogenic emission of greenhouse gases notably carbon dioxide, could lead to the irreversible melting of the polar ice and significant increases in global mean temperature. One of the mitigating strategies that can be carried out on a larger scale is the capture and geological sequestration of this gas.

Notable among proven geological resources is deep unmineable coal seams. Geological sequestration in these systems has a value added advantage because of coal bed methane production which is a source of cleaner burning fuel than coal. Accordingly the injection of carbon dioxide to a coal seam for long term storage accompanied by the production of methane requires adequate knowledge of the two phase flow characteristics of the methane/brine and carbon dioxide/brine systems. The most important characteristics of the two phase flow are relative permeability and capillary pressure. The coal core was characterized by proximate and ultimate ASTM measurements, x-ray diffraction (XRD), and scanning electron microscopy (SEM) analyses. These analyses identify the existence of clay minerals in the coal structure, which shows that origin of coal formation was from swamp plants. These minerals were used to fill the pores and reduce the permeability.

Relative permeability and capillary pressure data for Sydney basin coal samples were collected. This study has also obtained pore size distribution and its indexes both from capillary pressure data and statistical methods based on the hyperbolic model of capillary pressure versus saturation data. The elaborate experimental design and precise measurements using capillary pressure unit (TGC-764) with a pressure control module makes the acquired petro-physical data a valuable asset for future carbon dioxide enhanced coal bed methane production.

LIST OF ABBREVIATIONS AND SYMBOLS USED

ECBM	Enhanced coal bed methane
GtC	Gigatonne carbon
SEM	Electron scanning microscope
XRD	X-Ray diffraction
A	Area (m^2)
C_A	Concentration (kg mol/m^3)
D	Fractal dimension
D_V	Diffusivity (m^2/s)
J_A	Molar flux of component A (kg mol/m^2)
K	Permeability (m^2) [1 $m^2 = 10^{12}$ Darcy]
K_{rw}	Relative permeability of wetting phase
K_{rnw}	Relative permeability of non-wetting phase
M_w	Wet weight (g)
M_d	Dry weight (g)
P_b	Bulk volume (m^3)
P_c	Capillary pressure (psi)
P_{in} and P_{out}	Inlet and outlet pressures (psi)
P_v	Pore volume (m^3)
$\frac{dP}{dx}$	Pressure gradient per length (Pa/m)
Q	Flow rate within porous medium (m^3/s)
Q_o and Q_w	Flow rate of non-wetting and wetting phases (cm^3/s)
R	Pore throat radius (micron)
Se	Effective saturation
S_r	Irreducible water saturation
S_w	Water saturation
T	Temperature ($°C$)
V_b	Bulk volume of coal core (m^3)
V_{mw}	Volume of mobile water (m^3)

V_o and V_w	Effluent volumes of oil and water respectively (cm^3)
X	Distance (m)
θ	Contact angle
$\sigma_{effective}$	Effective stress (psi)
$\sigma_{vertical}$	Vertical stress (psi)
γ	Interfacial tension (mN/m)
$\emptyset$	Porosity of core sample
ρ	Density (g/cm^3)
μ	Viscosity of fluid (Pa.S)
μ_w	Linear absorption coefficient of water (m^{-1})
μ_x	Linear absorption coefficient of x-brine (m^{-1})
λ	Pore size distribution index

ACKNOWLEDGMENTS

I would like to thank all the people who have helped me and inspired me during my master's study.

Special appreciation goes to my supervisor Dr. Michael J. Pegg for his supervision, advice, and guidance through the experimental and thesis works from initial to final level. It has been an honor to be his master student. I doubt that I will ever be able to convey my appreciation fully.

Many thanks go in particular to Dr. Stephen Kuzak and Dr. Dmitry Garagash my committee members. I am much indebted to Dr. kuzak for his understating and kindness and also using my committee's precious times to read this thesis and give their critical comments about it.

I would like to thank Mumuni Amadu, who as a good friend was always willing to help and giving his best suggestions. My research would not have been possible without his help.

I gratefully acknowledge Dean Grijm and Ray Dube for their extraordinary assistance and aid in drilling core samples and helping in assembling Capillary Pressure Unit. Without them I could never run my experiments.

Where would I be without my family? My parents deserve special mention for their inseparable support and devotion. My father, Reza Nourbakhsh, in the first place is the person who put the fundament of my learning character, showing me the joy of intellectual pursuit ever since I was a child. My Mother, Monir, is the one who sincerely raised me with her caring and gently love. I owe my deepest gratitude to my parents for their endless support and encouragement to pursue this degree.

Finally, I offer my regards and blessings to all of those who supported me in any respect during the completion of the project.

CHAPTER 1: INTRODUCTION

1.1 BACKGROUND

The consensus of climatologists is that the increasing levels of greenhouse gases in the atmosphere, especially carbon dioxide, are contributing to global warming (NRC, 2010). The main source of these emission are human activities particularly in industrial processes such as paper mills, chemical plants, cement plants, petrochemical plants and power plants that burn fossil fuel. The rate of these emissions into the atmosphere is 3.3 gigatonne carbon (GtC) per year, which is a considerable amount. Therefore, with this high rate of CO_2 emissions, the main challenge to mitigating global warming is to reduce the emissions of CO_2 into the atmosphere. The increasing rate of CO_2 emissions into the atmosphere is critical for Canada because Canada is among the countries which have been withdrawal from the Kyoto Accord. There are many approaches to mitigate these emissions. The most successful one is Carbon Capture and Storage (CCS). With CCS, carbon dioxide emitted by industrial plants is captured at the source. The captured CO_2 is transported in tankers or pipelines to injection sites. Subsurface geologic reservoirs consist of salt caverns, deep saline aquifers, depleted oil/gas reservoirs, oceans and deep unminable coal beds. Sequestration of CO_2 in deep unminable coal seams has a value added advantage, because by injecting CO_2, methane, which is adsorbed on the surface of the coal, will be extracted. The augmented methane production can be used to offset the cost of CO_2 injection (Anderson *et al*., 2003).

To evaluate a coal field's reliability and predict its performance, a comprehensive study on its petro physical properties such as porosity, capillary pressure, relative permeability and pore size distribution of the coal sample is important.

1.2 OBJECTIVES

The objectives of this thesis are to determine the petro physical properties of coal sample from the Sydney basin coal field as part of Dalhousie University's contribution towards enhanced coal bed methane research initiatives. Accordingly the following are the research objectives:

1- Carry out coal sample characterization using ASTM, SEM and XRD

2- Determination of pore and bulk volume of the core sample as well as determination of cleat porosity of sample to brine at laboratory and reservoir conditions.

3- Preparation of brine with the exact composition of Sydney coal field brine.

4- Capillary pressure measurements of coal sample for CO_2/brine and methane/brine systems at ambient and reservoir conditions and comparison of the results.

5- Determination of relative permeability of coal core sample for both CO_2/brine and methane/brine systems.

6- Determination of the pore size distribution index for both systems and comparison of results at laboratory and reservoir conditions.

This thesis consists of five sections. Chapter 2 summarizes the main sources of CO_2 and the concept of CO_2 sequestration in geological formations, previous studies about preparing coal core samples and different methods of determining relative permeability. It also presents previous research results regarding the relative permeability of different gases and liquids in coal samples at different conditions of pressure. Chapter 3 describes the experimental set up and explains the applied test procedure. Finally, chapter 4 presents the results of capillary pressure measurements, followed by conclusions and recommendations.

CHAPTER 2: LITERATURE REVIEW

2.1 GREENHOUSE GASES

There are some gases in the atmosphere known as greenhouse gases, which absorb infrared radiation from the earth's surface and emit them back to the earth's surface. As a consequence of this phenomenon, the earth's surface becomes warmer. The major gaseous contributors are CH_4, CO_2 and N_2O. This phenomenon is the cause of the global warming effect, which is one of the most challenging of today's issues. According to a recent forecast by Wallington *et al.*, (2004) CO_2 concentration in the atmosphere in 2001 was measured at 370 ppm and this is expected to increase annually by 1.5 ppm.

2.2 SOURCE OF CO_2

Atmospheric air contains 0.04% CO_2. Large quantities of CO_2 can also be found in the ocean. These CO_2 reservoirs: biosphere, atmosphere and deep ocean, constantly exchange CO_2. According to Wallington *et al.*, (2004), oceans emit approximately 90 GtC CO_2 and absorb 92 GtC each year. Scientists have used several techniques for estimating net CO_2 exchange between the oceans, biosphere and atmosphere. These studies have shown that 2.0 ± 0.8 GtC per year is removed by oceans, forests remove 0.5-0.9 GtC of CO_2 per year and human activities such as deforestation and industrial works such as paper mills, chemical plants, cement plants and petrochemical plants and power plants that burn fossil fuel emit 5.5 ± 0.5 GtC per year. As a result, CO_2 in the atmosphere is increasing at the rate of 3.3 ± 0.2 GtC per year (Wallington et al, 2004). Akinnikawe *et al.,* (2010) has mentioned that in a medium coal-fired power station with 500 MW capacity, 3 million tonnes of CO_2 will be emitted per year. With such high rates of CO_2 generation, the main challenge to mitigate global warming is to reduce emissions of CO_2 to the atmosphere. Various approaches have been considered to mitigate these emissions. One of the most successful approaches is carbon capture and sequestration (CCS). Using this approach, the CO_2, which is generated from industrial plants, is captured before entering the atmosphere. Then the captured CO_2 is transported with tankers or pipelines and at the end CO_2 is stored in subsurface formations. Subsurface formations consist of salt caverns, deep saline aquifers, depleted oil/gas reservoirs, oceans and deep unmineable coal beds (Akinnikawe *et al.*, 2010).

2.3 CO_2 GEOLOGICAL SEQUESTRATION

The objective of CO_2 sequestration in geological formation is to inject high pressure CO_2 into the formations to displace in-situ fluids. According to Price and Smith (2008), there are five basic mechanisms that can trap CO_2 and hold it in the formations. These mechanisms are classified as structural, stratigraphic, residual, solubility and mineral trapping.

In stratigraphic trapping, CO_2 is trapped under an impermeable caprock that prevents CO_2 migration. Structural trapping occurs when impermeable layer of rock move along the fault or fold lines. Therefore, these impermeable layers prevent CO_2 from escaping. In residual trapping, CO_2 is injected into porous formations. Formation liquid is moved as CO_2 is displaced along the porous medium. The formation liquid replaces it. Thus, some immobile CO_2 is trapped in the formation. Generally, capillary forces in the formations trap CO_2 in the rock pores. In solubility trapping, as CO_2 is dissolved in residual saline formation liquid, became denser than the formation fluid and moves to the bottom of the formation. This movement makes trapping more secure over a long period of time. The last mechanism is mineral trapping. In this mechanism, CO_2 is dissolved in formation brine and chemical reactions bind it to the rocks and stabilize it (Price and Smith, 2008).

2.4 GEOLOGICAL STORAGE OF CO_2

2.4.1 DEEP SALINE AQUIFER

One of the advantages of using deep saline aquifer is that there a lot of them in nature and they occur in all kind of sedimentary basins. Their global capacity is approximately in the range of 1000 to 10000 Gt. Therefore they can store large approximately 100 years' worth of CO_2 emissions (Rapaka, 2009). For sequestering CO_2 in saline aquifers, supercritical CO_2 is injected into the formation to displace brine. For this purpose, a minimum depth of 800 meters is needed to maintain a sustainable supercritical regime for CO_2 and avoid its separation into liquid and gas during injection (Izgec *et al.,* 2005). To determine aquifer suitability for sequestration, thorough studies on the effect of temperature and pressure on displacement characteristics and relative permeability should be done (Bennion and Bachu, 2006). Examples of using saline aquifers for CO_2 sequestration are the Sleipner project of Statoil Company in Norway and in the near future, Shell in Alberta, Saskatchewan, will begin to operate sequestration CO_2 in aquifers (CCST @ MIT, 2011).

2.4.2 DEPLETED GAS/OIL RESERVOIRS

In this process, CO_2 is injected into the pore spaces of depleted gas/oil reservoirs. In some cases this injection could increase the gas/oil production, which is known as enhanced recovery. The process of enhanced recovery has been a common procedure in petroleum fields for over 30 years (Price and Smith, 2008). The advantage of using depleted reservoirs for CO_2 sequestration is that the geological information obtained during exploration and production stages of the reservoir is available. The major disadvantage of this process is that injected CO_2 could escape from wells, if the wells are not sealed properly. One of the on-going CO_2 sequestration projects in depleted reservoirs, which are operated by BP Company, is in the Salah project in Algeria (CCST @ MIT, 2011).

2.4.3 OCEANS

Atmospheric CO_2 dissolves and mixes into oceans and CO_2 sequestering occurs naturally every day. CO_2 sequestration in oceans has some advantages over sequestration in subsurface formations. For instance, in this process there is no need to maintain physical trapping. To sequester CO_2 in oceans, liquid CO_2 is injected to depths of more than 2743 m (9000 ft). In this depth CO_2 has higher density than the water in the upper layers.

Hence, CO_2 is trapped in the injected depth by buoyancy trapping (Ghorbani, 2012). Unlike wide studies about the technical feasibility of sequestrating CO_2 in oceans, not a lot of exploration has been done about its ecological implications. Disruption in marine ecological processes and degradation of the ecosystems are identified as its potentially serious impacts (Johnston and Santillo, 2002).

2.4.4 DEEP UNMINEABLE COAL SEAMS

The surface of coal has a high affinity to adsorb CO_2. During CO_2 injection, due to preferential adsorption of CO_2 over methane, CO_2 is adsorbed on the coal surface and trapped methane in the coal matrix is released. The advantage of this method is the increase of methane production from coal seams. This procedure of methane production is called, enhanced coal bed methane (ECBM). The global capacity for sequestering CO_2 in coal seams is estimated to be in the range of 15 to 200 Gt CO_2 (Rapaka, 2009).

2.5 COAL BED METHANE

In the process of coalification, where heat and pressure transformed organic matter like peat and wood to coal, large amounts of methane were also produced. In shallow surface coal seams methane usually escapes to the atmosphere but in deeper coal seams more methane is produced and trapped in the coal matrix due to exposure to higher pressure and temperature during formation. There are three different ways to recover coal bed methane. First, 50% of methane could be recovered by depletion of reservoir pressure. In the second method, hydraulic pressure is used to improve recovery but due to the low permeability of CBM, more wells have to be drilled, which is not economically efficient. The third way is to inject CO_2 or nitrogen to displace methane, which is called CO_2 /N_2 enhanced coal bed methane. In this method, more than 90% of the methane could be recovered and this approach has the advantage of storing CO_2 in to these formations (Gale and Freund, 2001).

2.5.1 COMPARISON BETWEEN CONVENTIONAL GAS RESERVOIRS AND CBM

CBM is considered an unconventional natural gas. Natural gas is absorbed on the surface of the coal matrix. In some cases CBM cleats are 100% water saturated and therefore must be dewatered to produce coal bed methane. Table 2.1 shows the difference between conventional gas reservoirs and CBM (Aminian @ WVU)

Table 2.1 Difference between Conventional Gas and CBM (Aminian @ WVU)

Characteristics	Conventional Gas	CBM
Gas Generation	Gas is generated in the source rock and then migrates into the reservoir	Gas is generated and trapped within the coal
Gas Storage Mechanism	Compression	Adsorption
Structure	Pores and possibly randomly-spaced fractures	Uniformly-spaced cleats
Transport Mechanism	Pressure gradient (Darcy's Law)	Concentration gradient (Fick's Law), Pressure gradient (Darcy's Law)

2.5.2 COMPARISON OF OIL RESERVOIRS AND CBM

In the oil reservoirs, hydrocarbons are trapped by the overlying impermeable rocks, while in a CBM reservoir; gas is both produced and kept in the coal. Table 2.2 shows the comparison between coal bed methane and oil reservoir.

Table 2.2 Comparison of Oil Reservoirs and CBM (Ham, 2011)

Characterization	**Petroleum Reservoirs**	**CBM Reservoirs**
Permeability	Essentially constant (weak pressure function)	Depends on pressure
Porosity	Essentially constant (weak pressure function)	Depends on pressure
Rock structure	Relatively simple	Pores and micro-fractures
Wettability	Constant	Variable, can be pressure Dependent

2.6 FLUID FLOW IN COAL SEAMS

Fluid flow in coal seams is governed by the coal characteristics and properties of the flowing fluid. The most important properties required to understand flow in porous media are porosity, permeability and wettability. Fluid flow in coal is governed by porosity on two scales: (micropores within the matrix) and secondary or cleat porosity. When flow is controlled by primary porosity, Fick's Law governs fluids transport in the micropores of the coal matrix. Fluid flow in cleats (secondary porosity), is governed by Darcy's Law (Mavor, 2006).

2.6.1 FICK'S LAW

Fluid flow diffuses in micropores of coal matrix and is defined by Fick's Law. Fick's law relates mass transport within the coal matrix by correlating mass transfer to the concentration gradient. Fluid flows from high to low concentration (Smith, 2008). Fick's law is defined as:

$$J_A = - D_V \frac{dC_A}{dx} \quad (2.1)$$

Where

J_A = Molar flux of component A [mole/m^2 s]

D_V = Diffusivity [m^2/s]

C_A = Concentration [mole/m^3]

X = Distance [m]

2.6.2 DARCY'S LAW

Fluid flow in cleats is governed by Darcy's Law. Pressure gradient is the driving force for this made of transport. The unit of permeability "k" is Darcy. To use Darcy's Law for permeability measurements, two conditions should be maintained; the fluid flow regime should be laminar and there should not be any reaction between the rock structure and flowing fluid (Ahmed, 1946). Darcy law in SI units is given by:

$$q = -\frac{kA}{\mu}\frac{dP}{dx} \qquad (2.2)$$

Where

q = Flow rate within porous medium [m^3/s]

k = Permeability [m^2] [1 m^2 = 10^{12} Darcy]

A = Area [m^2]

μ = Viscosity of fluid [Pa.S]

$\frac{dP}{dx}$ = Pressure gradient per length [Pa/m]

2.7 PETRO PHYSICAL PROPERTIES OF COAL

Coal characteristics and properties of the flowing fluid determine the fluid flow in coal seams. As mentioned above, the most important petro physical properties required to understand fluid flow in coal are porosity, permeability and wettability. Coal consists of a distribution of pore sizes that can be classified into three categories: microspores (smaller than 2 nm), mesopores (in range of 2 to 50 nm) and macrospores (more than 50 nm). The difference between fluid flow governed micro porosity and that governed by macro porosity explains the dual porosity characteristics of coal beds (Mavor, 2006).

2.7.1 PRIMARY POROSITY OF COAL BED METHANE

The micropores in a coal bed structure have diameters that vary from 0.5 to 1 nm. One gram of coal has a surface area more than 5000 m^2 (Dallegge and Barker, 2000). Diffusion governs the gas flow within the coal matrix. Generally it is assumed that water does not flow through coal micropores within the matrix (Van Krevelen, 1993). Therefore, transport of water in Coal seams resources occurs through secondary porosity systems in macropores (Mavor, 2006).

2.7.2 SECONDARY POROSITY

The secondary porosity or cleat porosity consists of cleats or fractures with apertures more than 10 µm and mesopores greater than 50 nm. There are three kinds of cleats; face cleats, butt cleats and joint cleats. Figure 2.1 shows the cleats in a coal structure. Face cleats are the fractures which are continuous through the bedding planes. Butt cleats end up perpendicular to the face cleats, while joint cleats are large fractures along coal bedding and in some cases cross through lithological boundaries. The secondary porosity of coal seam is usually in the range of 0.0004% to 6% (Mavor, 2006).

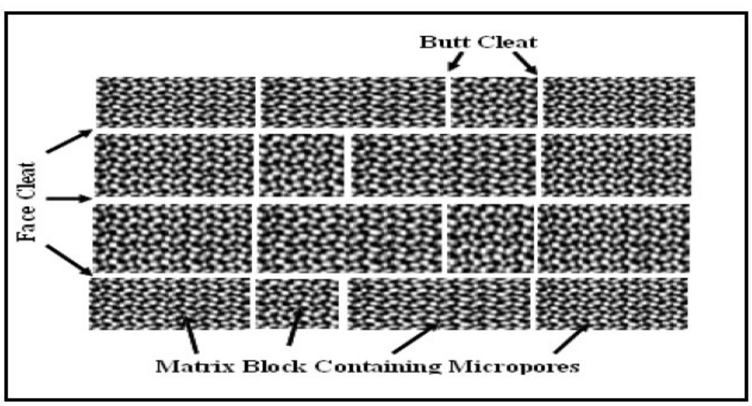

Figure 2.1 Cleats in coal structure (Harpalani and Chen, 1995).

2.7.3 PERMEABILITY

Permeability is a measure of the ease with which fluids are transferred through porous media and measured in Darcy. It is one of the important characteristics of coal that should be determined to ascertain if a field can start production or not. Since, if a field has a high permeability, fewer wells should be drilled for production. (Zhangxin, 1962).

Table 2.3 Classification of Rocks and their Range of Permeability (Zhangxin, 1962)

Classification	Permeability range (md)
Poor to fair	1-15
Moderate	15-20
Good	50-250
Very good	250-1000
Excellent	Over 1000

2.7.4 ABSOLUTE PERMEABILITY

Absolute permeability is calculated based on the flow rate through all the pores and cleats when the porous media is 100% saturated with one fluid. It was observed by Jones *et al.*, (1988) that coal seams, which are buried at great depths, have a low permeability due to the effect of overburden pressure on coal structure. Jones *et al.,*(1988) also stated in the USA, the absolute permeability of coal bed reservoirs range from 0.1 to 120 mD. In Australia this range is from 1 to 10 µD and in European counties this range varied from 1 to 50 µD (Jones *et al.,* 1988).

2.7.5 EFFECTIVE PERMEABILITY

The ability of one fluid to pass through a porous medium in the presence of other fluids is called effective permeability. effective permeabilities to oil, gas and water (k_o, k_g, and $k_{w)}$, can be easily determined in the laboratory Water saturation affects effective permeability. Therfore, prior to effective permeability measurments, it is important to determine water saturation (Ahmed, 1946).

2.7.6 RELATIVE PERMEABILITY

Relative permeability is a measure of the capacity of the coal to transport one fluid, when more than one fluid is present. At a particular saturation, relative permeability is determined when effective permeability of each phase is divided to the absolute permeability.

If water, oil, and gas flow through the medium simultaneously, then for each phase the relative permeability is described as $K_{rw,}$ K_{ro} and K_{rg}. As the value of effective permeability varies from 0 to "k", the value of relative permeability goes from 0 to 1(Ahmad, 1946). There are two methods to measure relative permeability: steady-state (Penn State) and unsteady-state methods.

2.7.6.1 STEADY-STATE

To measure relative permeability using the steady state method at a specific saturation, two immiscible fluids flow through a coal core samples at constant pressure, until the pressure gradient became stable and equilibrium is reached. By measuring the produced volume for the fluids, the pressure gradient and the flow rates and using Darcy's law, relative permeability can be determined. This process is repeated with different flow rates and different saturation rates. One of the disadvantages of the using steady state method is that it takes long time until equilibrium is achieved but the results are more accurate and reliable than the unsteady state (Honarpour and Mahmood, 1988). Figure 2.2 shows a schematic of steady state method.

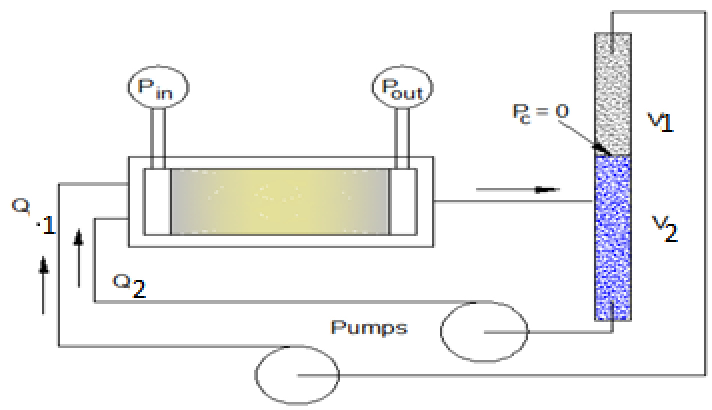

Figure 2.2 Schematic of relative permeability measurements with the steady state method (Lenormand, 2006). P_{in} and P_{out} = Inlet and outlet pressures [psi], P_c = Capillary pressure [psi], Q_1 and Q_2 = Flow rate of non-wetting (fluid 1) and wetting (fluid 2) phases [cm^3/s] , V_1 and V_2 = Effluent volumes of fluid 1 and 2 respectively [cm^3]

2.7.6.2 UNSTEADY STATE

In order to determine relative permeability using the unsteady state method, the core sample should be first saturated with in-situ fluid and then a displacing fluid is injected through the core sample continuously with constant flow rate until equilibrium is reached. One of the advantages of this method is that it is not time consuming (Honarpour and Mahmood, 1988) and one of the disadvantages of this method is that in a water/gas system, if the core sample has low permeability to water, further reduction of water saturation is extremely difficult. Therefore gas permeability of core sample would be reduced. Figure 2.3 shows a schematic of unsteady state measurements of relative permeability.

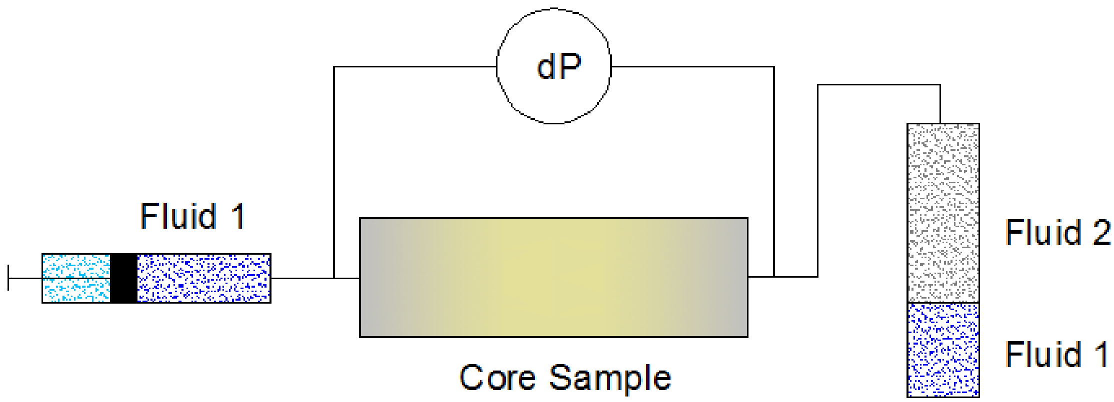

Figure 2.3 Schematic of unsteady state measurements of relative permeability (Lenormand, 2006)

By monitoring produced volumes of both fluid 1 and fluid 2 as a function of time, various mathematical models like the Buckley and Leveret model (1942) can be used to determine relative permeability as a function of water saturation. According to (Ahmad, 1946), the Buckley and leveret model can be used to determine of relative permeability. In order to find relative permeability with this model, fluid flow is calculated by using Darcy's law:

$$q_g = -\frac{AK_g}{\mu_g}\left(\frac{\partial P_g}{\partial x} + \rho_g g \sin\alpha\right) \tag{2.3}$$

$$q_w = -\frac{AK_w}{\mu_w}\left(\frac{\partial P_w}{\partial x} + \rho_w g \sin\alpha\right) \tag{2.4}$$

Where

q_g = Gas flow rate [m^3/S]

q_w = Water flow rate [m^3/S]

A = Area [m^2]

K_g = Effective permeability to gas [m^2] [1 m^2 = 1.0132×10^{12} Darcy]

K_w = Effective permeability to water [m^2]

μ_g = Viscosity of gas [Pa.S]

μ_{w} = Viscosity of water [Pa.S]

P_g = Pressure of gas [Pa]

P_w = Pressure of water [Pa]

α = Angle of inclination [degrees]

Capillary pressure is defined as:

$$P_c = P_{nw} - P_w \tag{2.5}$$

Therefore:

$$\frac{dP_c}{dx} = \frac{\partial P_g}{\partial x} - \frac{\partial P_w}{\partial x} \tag{2.6}$$

Rewriting Equation 2.3 and 2.4:

$$\frac{\partial P_g}{\partial x} = - \frac{\mu_g q_g}{AK_g} - \rho_g \text{ g} \sin \alpha \tag{2.7}$$

$$\frac{\partial P_w}{\partial x} = - \frac{\mu_w q_w}{AK_w} - \rho_w \text{ g} \sin \alpha \tag{2.8}$$

Substituting Equation 2.7 and 2.8 in Equation 2.6 :

$$\frac{\partial P_c}{\partial x} = - \frac{\mu_g q_g}{AK_g} - \rho_g \text{ g} \sin \alpha + \frac{\mu_w q_w}{AK_w} + \rho_w \text{ g} \sin \alpha \tag{2.9}$$

It should be noted that:

$$q_t = q_w + q_g \tag{2.10}$$

Substitution of Equation 2.10 in to Equation 2.9 yields:

$$\frac{\partial P_c}{\partial x} = - \frac{\mu_g (q_{t-} q_w)}{AK_g} + \frac{\mu_w q_w}{AK_w} + \Delta\rho g \, sin\alpha \tag{2.11}$$

Dividing both sides of Equation 2.11 by ($\frac{\mu_g q_t}{AK_g}$), f_w can be obtained:

$$f_w = \frac{1+\frac{AK_g}{\mu_g q_t}(\frac{\partial P_c}{\partial x} - \Delta\rho g\, sin\alpha)}{(1+\frac{K_g\,\mu_w}{K_w\,\mu_g})} \quad (2.12)$$

Where

f_w = Water cut [bbl/bbl]

k_{rw} ,K_{rg}= Relative permeability for water and gas

μ_w ,μ_o = Viscosity of water and oil [cP]

A = Area [ft^2]

q = Total flow [bbl/day]

g = Gravitational acceleration coefficient [ft/sec^2]

$\Delta\rho$ = Difference between water and oil in density [g/cm^3]

α = Dip angle

Water cut is the ratio of produced water compare to the volume of total liquids produced. If the apparatus that is used for this calculation simulate the reservoir horizontally, the equation is reduced to:

$$f_w = \frac{1}{(1+\frac{K_g\,\mu_w}{K_w\,\mu_g})} \quad (2.13)$$

2.7.7 EFFECT OF STRESS (PRESSURE) ON COAL PERMEABILITY

During two phase flow in the coal cleats, the water saturation of the coal seam and the cleat width will change due to decrease in CBM reservoir pressure and this will lead to changes in permeability (Mavor, 2006).

According to GRI, (1996), the effective stress is defined as below:

$$\sigma_{effective} = \sigma_{vertical} - P \quad (2.14)$$

Where,

$\sigma_{vertical}$ = Vertical stress [psi]

P = Pore pressure [psi]

Harpalani and Schraufnagel (1990) reported that by decreasing coal seam pressure, according to previous equation, the effective stress would increase, consequently closing the cleats, resulting in decreased permeability.

2.7.8 WETTABILITY`

Wettability is defined as the ability of a liquid to spread over the surface of a solid when immiscible fluids flow through porous media. Ahmed (1946) stated that both wetting and non-wetting phases flow through different paths in the porous media. The wetting phase occupies small pores of a porous medium. These small pores don't have a major impact on the fluid flow in porous media; therefore, small wetting phase saturation will slightly reduce the permeability of the non-wetting phase while the non-wetting phase tends to occupy large pores, which are the main contributors to fluid flow. Therefore, when the non-wetting phase has low saturation, it will significantly reduce the wetting phase permeability (Ahmed, 1946).

2.7.9 CAPILLARY PRESSURE

Capillary pressure is one of the important parameters that determine the behaviour of a porous medium in the presence of two immiscible fluids. When a single capillary with a variation in its cross section is filled with the wetting phase (this happens when the sample is saturated) and the non-wetting phase is injected at atmospheric pressure, because the pressure difference is zero, it can't penetrate into the capillary. The pressure must be increased to allow this to happen. Capillary pressure is defined by Equation 2.15:

$$P_c = P_{nw} - P_w = \frac{2\gamma\cos\theta}{r} \qquad (2.15)$$

Where

P_c = Capillary pressure [psi]

P_{nw} = Non-wetting phase pressure [psi]

P_w = Wetting phase pressure [psi]

θ = Contact angle [degrees]

r = Pore throat radius [microns]

γ = Interfacial tension [mN/m]

The non-wetting phase penetrates the pore until it reaches the local minimum pore radius, which is called the pore throat. To continue penetration in the narrower pore throat, capillary pressure must be increased. Drainage is the process by which a non-wetting phase displaces a wetting phase (Dullien, 1991).

Brook and Corey (1996) conducted a number of drainage capillary pressure experiments and found out that log-log diagram of effective saturation and capillary pressure is linear when the data for water saturation above 0.85 are omitted. By extrapolating this line, the intercept indicates the breakthrough capillary pressure (P_b) and slope is the reciprocal of pore size distribution index ($1/\lambda$). Based on their experiments, Brook and Corey, (1996) developed an equation to determine relative permeability from capillary pressure and corresponding saturation data.

$$S_e = \left(\frac{P_b}{P_c}\right)^{\lambda} \qquad (2.16)$$

Where

P_c = Capillary pressure [psi]

P_b = Break through capillary pressure [psi]

S_e = Effective saturation

λ = Pore size distribution index

According to Brook and Corey theory, λ is a positive value greater than zero. The value of λ depends on the pore structure of the media. Its value is small when the medium has a wide range of pore sizes and its value is large when the medium has relatively uniform pore size.

Breakthrough capillary pressure is the capillary pressure at which the non-wetting phase fluid (oil or gas) just begins to enter the porous medium containing the wetting phase fluid (formation brine). It also shows the diameter of the largest pore in the porous medium since capillary pressure is related to pore radius and interfacial tension. Effective saturation is given by Equation 2.1:

$$S_e = \frac{S_w - S_r}{1 - S_r} \tag{2 -17}$$

Where

S_r = Irreducible water saturation

S_w = Water saturation

Using the data from their experiments Brook and Corey, (1996) formulated an equation to find relative permeability with capillary pressure data.

$$K_{rw} = (S_e)^{\left(\frac{2+3\lambda}{\lambda}\right)} \tag{2.18}$$

$$K_{rnw} = (1-S_e)^2 \left(1-S_e^{\frac{2+\lambda}{2}}\right) \tag{2.19}$$

Where

K_{rw} = Relative permeability of wetting phase

K_{rnw} = Relative permeability of non-wetting phase

To correlate the obtained laboratory data to the reservoir condition, following procedure should be done. According to Seidle, (2011), with definition of compressibility, Bulk volume and pore volume at reservoir condition is calculated.

$$C_B = \frac{1}{V_{Bi}} \frac{dV_B}{dp} \tag{2.20}$$

$$V_{B(res)} = V_{Bi} - dV_B \tag{2.21}$$

$$V_{Pi(res)} = V_{Bi} \times \varphi_{res} \tag{2.22}$$

Where,

φ_{res} = Porosity at reservoir condition

V_{Bi} = Initial bulk volume [cm^3]

$V_{Pi(res)}$ = Pore volume at reservoir condition [cm^3]

C_B = Cleat bulk compressibility [psi^{-1}]

By having porosity and bulk volume at reservoir condition, pore volume at reservoir condition is obtained. By having these data, saturation data at laboratory condition can be correlated to the reservoir condition. To determine capillary pressure at reservoir condition Equation 3.8 can be used. Therefore, by plotting log-log of capillary pressure versus saturation, pore size distribution index at reservoir is determined.

There are four different methods to measure capillary pressure:

1) Porous diaphragm
2) Mercury injection
3) Centrifugal method
4) Magnetic resonance method

2.7.9.1 POROUS DIAGRAM

In this method, a porous plate is used with core sample. Both the core sample and the porous plate should be saturated with the same fluid and placed in the core holder. When the gas is injected, it displaces the liquid from the core and the porous plate allows this displaced liquid to go into the outflow. One of the advantages of this method is its accuracy, although it is very time consuming and the range of capillary pressure is limited to the displacement pressure of the porous plate (Dullien, 1991).

2.7.9.2 MERCURY INJECTION

In this method high pressure mercury is injected in to the core sample to displace fluid. One of the advantages of this method is that it takes only minutes to get the result and it covers a high range of capillary pressure but mercury is destructive and the core can't be used again (Dullien, 1991).

2.7.9.3 CENTRIFUGAL METHOD

In this method a core sample is first saturated and then placed in the core holder. Different rotational speeds can be set when a gas is injected to the core holder to displace fluids. Then, the volume of displaced fluid is measured. This method is reaches the equilibrium very quickly but one of its disadvantages is that complex analysis required, which can lead to calculation errors (Hassler and Brunner, 1945).

2.7.9.4 MAGNETIC RESONANACE METHOD

In this method, amounts of hydrogen in the sample are detected. The life time of detected signal depends on the environment of the hydrogen. The signals from hydrogen in free water decay slower than the signals of hydrogen in oils. In this method the magnetic field is altering linearly and a magnetic field gradient is created. Therefore, a variety of pulse sequence is obtained but because these data are dependent on many factors such as pore size, fluid diffusion and so on, analysis of the results is difficult (Green, 2007).

In this research capillary pressure was determined using the porous plate method.

2.7.10 PORE SIZE DISTRIBUTION

The pore size distribution can be obtained if the system consists of a wetting phase and non-wetting phase. In that case, contact angle is assumed to be the same for all the pressures. The capillary pressure required to let the non-wetting phase into the pores, is a function of the largest pore throat. Finding the distribution of pore size is an important for analyzing the properties of porous media. Equation 2.23 gives the largest pore size in porous systems:

$$r_i = \frac{2\sigma}{P_c} \tag{2.23}$$

Ritter and Drake (1945) develop the theory of a non-wetting phase invading a porous medium. This theory was modified for reservoir rocks by Burdin et al.,(1950). Equation 2.24 shows the surface area distribution of pore ($D_{(}r_i)$):

$$D(r_i)dr = dV_p = V_p\, dS_w \tag{2.24}$$

By considering cos θ = 1, in the differentiating Eq. 2.23:

$$dr = \frac{r^2}{2\delta}\, dP_c \tag{2.25}$$

By substituting Eq. 2.25 into Eq. 2.24:

$$D(r_i) = \frac{P_c V_p}{r}\frac{dS_w}{dP_c} \tag{2.26}$$

The largest of pore throat is invaded at $S_w = 1$, where the $r_{max} = 2\partial/P_c$, and the minimum pore size occurs at irreducible water saturation. Donaldson *et al.* (1991) found that capillary pressure and saturation data are best fitted by a hyperbolic function.

$$(P_c)_i = \frac{A+BS}{1+CS} \tag{2.27}$$

To find dS_w/dP, they stated that a least square solution of a hyperbolic function represented all capillary pressure curves as below:

$$d(P_c)_i = \frac{B+AC}{(1+CS)^2}\, dS \tag{2.28}$$

2.8 FRACTALS

A fractal is a shape that is similar to the whole. The concept of fractals is based on self-similarity. Self-similarity means that patterns appear in all scales of observation. For example, to measure the length of a coastline with a yardstick, it was observed that one solid number as the length of the coastline is meaningless without specifying the scale of measurement because the shorter the yardstick gets, the measured length of coast line increases. Mandelbrot (1983) found that the length of the coastline $L(\sigma)$ is a function of the length of the yardstick (σ), which is defined by power law:

$$L(\sigma) = F(\sigma)^D \tag{2.29}$$

Where

D = Fractal dimension

F = Constant

Over the past decade, the concept of a fractal has been widely used in the analysis of processes in nature especially including flow through porous media. It has been found by Deinert *et al*. (2008) that a pore space is a fractal structure. As we know, pore space is a fundamental property of porous media, in which two phase flow occurs. Therefore, all the properties that are related to pore space exhibit fractal behavior. In this regard, Katz and Thompson (1985) stated that porosity is a fractal property. Pfeiner and Aveiner (1983) found that pore interfacial intension also shows fractal behaviour.

Capillary pressure and pore volume are proportional to pore radius. Therefore they should exhibit fractal behaviour. The relationship between capillary pressure and water saturation obeys the power law function (Deinert *et al*., 2008).

Similar studies have been done by Turcote *et al.* (1986) and Tyler and Wheatcraft (1989) to show that particle size distribution exhibits fractal behaviour and is defined by the power law. In this regard, in the Eq. 2.29, $L(\sigma)$ is the number of the particle and the measurement scale σ is the particle diameter.

2.9 COLLECTION AND PREPARATION OF A COAL SAMPLE

There are various methods for preparing coal samples for performing flow experiments. The highly friability of coal make it extremely difficult to obtain samples. Puri *et al*. (1991) used 3 ft. length core samples for determining the relative permeability of Warrior Basin and San Juan Basin coal by using well logs. The depth of the coal was measured. They kept the samples horizontally in a water container to prevent them from breaking. They found that if the core has less ash concentration, it is more light weight and has more cleats. Before running the flow test, in order to minimize breakage of the core, small cracks on the surface of the core were filled with epoxy wrapped with Teflon tape and covered with heat-shrink tubing. X-ray scans were used to select the best core sample with more cleats. Puri *et al*. (1991) also found that core samples with diameters in the range of 2.5 to 3.5 inch produce more reliable results than the smaller ones because permeability of coal is based on cleats and pore matrix; therefore small cores are not able to represent coal seam characteristics.

Taber *et al*. (1974) used two different coals for their relative permeability studies. The first sample from Pocahontos was friable and the second one was a less friable coal from Pittsburgh. At first they cut the coal from the mine with a diamond blade and then cylindrical cores of 1½ inch in diameter were drilled perpendicular to the bedding deposition plates. They coated the samples with epoxy to protect the rubber sleeve from being ruptured when confining pressure is high. Then they used a grinder to flatten the core's two sides.

Gash (1991) used different coals from different depths with four different dimensions (ratio of length to diameter varied from 0.83 to 1.85) to measure the effect of different cleat structures on the permeability of San Juan Basin and Warrior Basin coals. He used heat shrink tubing and Teflon wraps for coating the samples.

Hyman *et al*. (1992) and Gash (1991) used San Juan Basin and warrior Basin coal samples for capillary pressure and permeability measurements. Hyman *et al*. (1992) kept the core samples in brine containers and added biocide to the brine to preserve them longer.

Paterson *et al*. (1992) studied the permeability of Australian coals. They used low permeability dull bands coal instead of high fractured bright bands coal; their reason for this selection was their better aggregation during transportation. Paterson *et al*., (1992) used two cores with the length of 2 and 4.7 inch and coated them with heat shrink tubing.

Robertson and Christiansen (2007) gathered their coal samples from Wyoming and Utah coal mines. The sample from Utah was taken fresh from an underground coal mine, sealed with tape to prevent it from oxidation with air and then kept in a container of de-ionized water. The other sample from Wyoming was about 1 ft^3 and kept in water. Then, Robertson and Christiansen (2007) took coal samples from the water and drilled their samples with a 2 inch diameter and wrapped them with aluminum foil. The flowing fluid used for their experiment was nitrogen.

2.10 CLEAT POROSITY MEASURMENTS

As mentioned earlier, the porosity of coal is a function of the porosity of its matrix and cleats. Measurement of porosity is important in order to obtain saturation in relative permeability and capillary pressure measurements (Gash, 1991). Different methods have been proposed by different researchers to measure porosity and some are discussed below.

Taber *et al.* (1974) measured the coal porosity with gas and water. They used a helium porosimeter to measure the porosity of coal using gas. To determine the porosity of coal using water, they dried the coal samples and then used water imbibition for 48 hours. According to their measurements, for water saturation between 0.4% and 1.1% coal porosity to helium varied between 2.6% and 8.6%. They also found that helium, which is a non-adsorbing gas, flows through the coal matrix but water can only flow through cleats. In other words, in 100% water saturation, gas saturation in coal is not zero. Taber *et al*. (1974) mentioned that coal samples that were dried at 90 °C had more porosity using water and gas.

Puri *et al.* (1991) used sodium iodide and x-ray absorption to trace and monitor irreducible water saturation and calculate coal porosity. In the first step, a coal sample was 100% saturated with brine and then linear x-ray scan was used to determine how x-ray decreases through the sample (I^1). In the second step, six Litters of helium flowed through the sample for four hours and then another x-ray scan was obtained along the core sample (I^2). In the third step, 150 grams of sodium iodide was dissolved in one liter of water to produce brine. This brine was injected into the coal samples for 24 hours to displace helium. Again a x-ray scan was obtained through the sample (I^3). In the last step, helium flowed through the sample for four hours and then a x-ray scan along the sample was obtained (I^4). By having these x-ray data, the irreducible water saturation was determined using Lambert's law:

$$\mathrm{I} = \mathrm{I_O} \exp\left[-\mathrm{c} - \mu_0\, \emptyset D\right] \tag{2.30}$$

$$\ln(\mathrm{I}^1) - \ln(\mathrm{I}^3) = -\left(\mu_w - \mu_x\right) \emptyset D \tag{2.31}$$

$$\ln(\mathrm{I}^2) - \ln(\mathrm{I}^4) = -\left(\mu_w - \mu_x\right) S_{wr} \emptyset D \tag{2.32}$$

Where

C = Constant

μ_o = Linear absorption coefficient of fluids in pore space [m^{-1}]

D = Diameter of core sample [m]

$\emptyset$ = Porosity of core sample

I = Intensity of X-ray beam

μ_w = Linear absorption coefficient of water [m^{-1}]

μ_x = Linear absorption coefficient of x-brine [m^{-1}]

To calculate effective porosity, the volume of water in the cleats after the injection of brine in the helium saturated sample was measured (Puri *et al.*, 1991). Effective porosity is calculated with the equation below:

$$\emptyset_e = \frac{V_{mw}}{V_b} \tag{2.33}$$

Where

V_b= Bulk volume of coal core [cm^3]

V_{mw} = Volume of mobile water [cm^3]

$\emptyset_e$ = Effective porosity

According to Puri *et al*. (1991), the helium porosity that they obtained through the experiments was 21.2%. The water porosity of San Juan samples was 1.5% and for Warrior samples it was 1.9%.

In 1991, Gash dissolved lithium chloride in deionized water to determine cleat porosity with a tracer. First, he determined the cleat pore volume by measuring the total volume of displaced fluid minus the dead volume. Then he calculated the cleat porosity by dividing the cleat pore volume by the coal sample bulk volume. He also determined water porosity of the coal cleats by injecting helium into the water saturated coal sample. Water out flow was measured and divided by the core bulk volume. Table 2.4 shows the cleat porosity and water porosity of four samples that were used in this experiment.

Table 2.4 Cleat and Mobile Water Porosities in Coal Cleats (modified from Gash, 1991).

Core	A	B	C	D
Confining pressure (psig)	1000	450	450	450
Cleat porosity (%) by tracer test	1.6 ±0.3	0.9 ±0.2	0.8 ±0.3	1.2 ±0.7
Mobile water porosity (%)	1.1 ±0.1	0.9 ±0.1	0.6±0.1	1.0 ±0.3
Diameter (inch)	3.5	3.5	3.5	2.0
Length (inch)	3.3	3	4.3	3.7
L/D	0.94 < 1	0.86 < 1	1.23 > 1	1.85 > 1

2.11 MEASURMENT OF THE ABSOLUTE PERMEABILITY OF COAL

Taber *et al.* (1974) measured the absolute permeability of 35 Pocahontas and Pittsburg coal cores to air and water. To determine the absolute permeability to air, 200 psig and 400 psig were applied as overburden pressures. The absolute permeability of Pocahontas coal to air at 200 psig varied widely between 0 to 50 mD. The results of the Pittsburgh samples were similar. The absolute permeability at 400 psig varied between 0 to 0.01 mD. Taber *et al*. (1974) tried to measure absolute permeability of samples to water by applying an overburden pressure of 400 psig. The results of these experiments showed that water absolute permeability was less than air absolute permeability because the cores were saturated with water before the tests. Therefore, when the water was injected into the core, adsorbed water caused swelling and through further injection there was a reduction in water flow paths.

Gash (1991) obtained the absolute permeability to water four coal samples water when he applied 370 psig as an injection pressure and set the back pressure at 300 psig. He observed that absolute permeability decreases through continuous water injection over a period of two months.

Gash (1991) obtained the permeability with a reversed direction in fluid flow. There was an increase in permeability due to the fines migration along the sample. These fines were produced along the coal sample when the sample was mined and exposed to atmospheric pressure at the surface. He also measured the absolute permeability of samples to deionized water. He observed a rapid decrease in permeability within 24 hours. In his experiments he tried to find out the effect of cleat orientation on permeability. For this purpose, he applied the previous pressure, 370 psig, as an injection pressure and set 70 psig as a pressure drop along the core. He found that the greatest of permeability was obtained when the flow was parallel to the coal bedding. He also repeated his experiments with overburden pressures between 500 psig to 1000 psig and observed that the permeability decreases by five orders of magnitudes.

2.12 MEASURMENT OF THE RELATIVE PERMEABILITY OF COAL

In order to measure the relative permeability of Pocahontas and Pittsburgh coal samples to air and water, Taber et al. (1974) used a steady-state method for imbibition and drainage. They found that steady state method was not suitable for measuring water permeability in drainage cycles due to the increase of water saturation during the tests. Therefore water relative permeability in drainage cycles was calculated using data from air permeability tests and using the Corey method. Taber *et al.* (1974) used drainage and imbibition data to plot permeability curves. It was understood from the curves that the effective permeability to gas in imbibition was smaller than the drainage. They also stated that gradual changes in permeability are due to distribution of pore size along the core sample. In this regard, severe changes in permeability occurs when fluids passes through large cleats. From the permeability curves, they also found that effective permeability is lower than absolute permeability. Figure 2.4 shows the effective permeability vs. saturation. The solid lines refer to the first run and the dash lines referred to re-run tests.

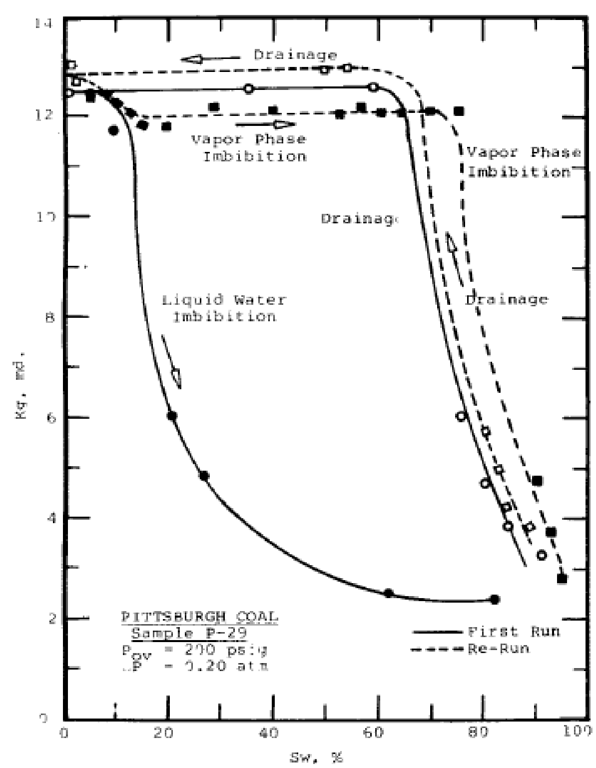

Figure 2.4 Gas/water effective permeability vs. saturation (Taber *et al.*, 1974).

Puri *et al.* (1991) used the unsteady and state method to determine the relative permeability to gas and water of coal core samples. They collected their samples from Warrior Basin and San Juan Basin. They first conducted a pre-test in which gas was eliminated from the coal sample and the confining pressure was set at 450 psig and the back pressure at 300 psig. Water at 120°F was injected into the core sample for eight hours to release adsorbed methane from the coal matrix. This process continued until stable permeability was reached. For obtaining relative permeability, Puri *et al.* (1991) injected helium with a constant inlet pressure into the core sample. Water and gas were separated in the outlet flow and monitored carefully with a mass flow meter. x-ray scans were taken during the experiment. With the obtained data, irreducible water saturation and relative permeability were calculated. Puri *et al.* (1991) stated that providing a constant confining pressure during the test and at the water/gas separator is essential and the data should be gathered during the first 15 minutes of the test. Puri *et al.* (1991) plotted relative permeability curves and compared the porosity and relative permeability of both samples. Figure 2.5 and figure 2.6 show the relative permeability results of the San Juan and Warrior Basins.

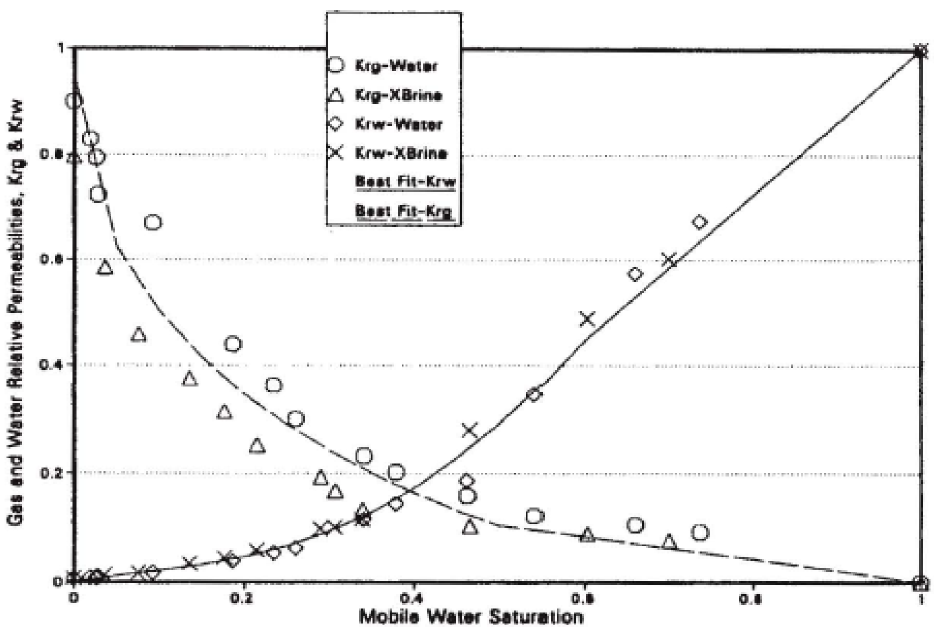

Figure 2.5 Laboratory measurements of San Juan Basin coal (Puri *et al.*, 1991)

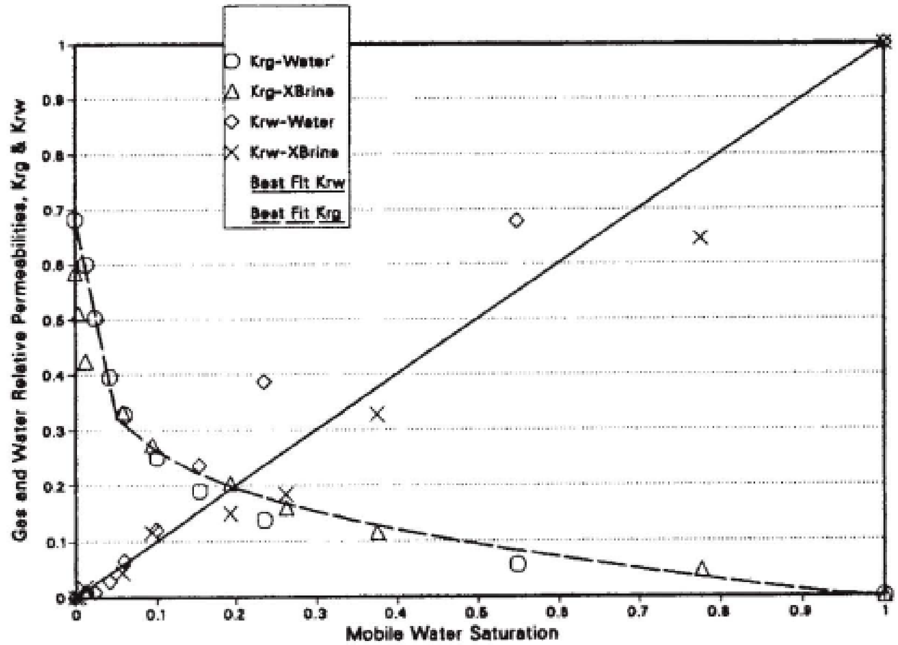

Figure 2.6 Laboratory measurements of Warrior coal core samples (Puri*et al.*, 1991).

Gash (1991) measured the relative permeability of coal samples from Warrior Basin using the steady state and unsteady state methods. He stated that in the unsteady state method, accurate measurements of dead volume are very important because these measurements always have error due to the low porosity of coal samples. He used the JBN method for different pressures to obtain relative permeability curves. In steady state relative permeability measurements, he injected sodium iodide for nine days and used x-ray scans to monitor sodium iodide adsorption along the core sample to obtain water saturation. In his measurements he assumed that all cross sections in the core were uniformly saturated. Gash (1991) plotted relative permeability curves. He used the data for the absolute permeability to water for base permeability in his calculations. From these plots he observed that the curves obtained from both steady state and unsteady state methods were similar. Figure 2.7 shows this similarity and also the crossover of gas/water relative permeability in both models is at the same point.

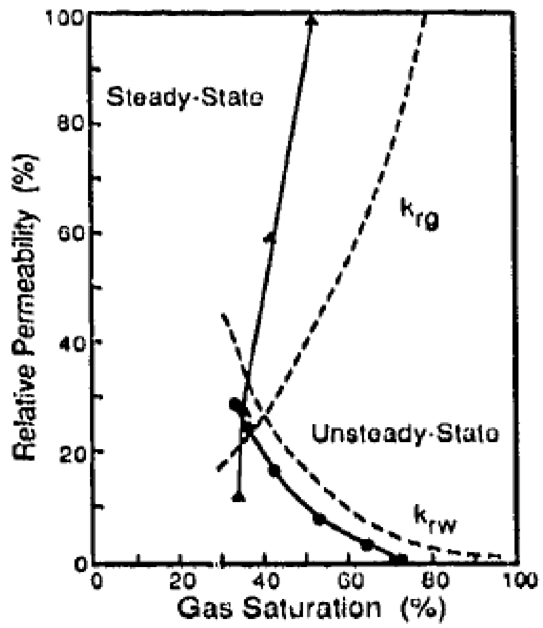

Figure 2.7 Gas/water relative permeability measurements with steady state and unsteady state models (Gash, 1991)

Hyman *et al.* (1992) measured the relative permeability of coal samples from Black Warrior Basin with the steady state and unsteady state method. In measurements made at steady state, different ratios of gas and water injected into the coal core samples until equilibrium was reached. The fluid saturation was measured with x-ray scans. One of the advantages of this method is its suitability for carbonate and clastic samples and one of its disadvantages is that it requires a long time long to reach the equilibrium state. To use unsteady state measurements, the core sample was first vacuum saturated with brine for several minutes and then was placed in the core holder; brine was injected for 24 hours while the back pressure was set at 300 psia. The absolute permeability to brine was determined this way. Hyman *et al.* (1992) injected helium with the constant pressure to displace brine until a stabilized condition was reached. One of the disadvantages of using the unsteady state method is that one needs to obtain cleat porosity in order to find the correlation between saturation and pore volume. Hyman *et al.* (1992) used the JBN model to obtain relative permeability. They plotted the measured relative permeability from methods and observed similarity between them. They explained that these similarities are due to coal problems and fines migration.

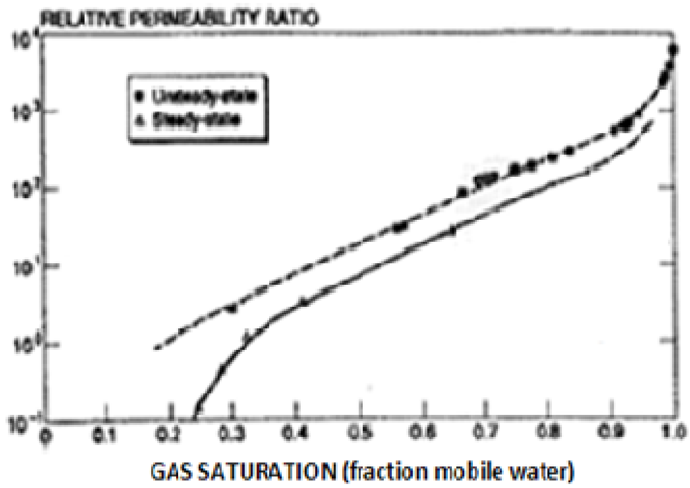

Figure 2.8 Laboratory relative permeability measurements from steady state and unsteady state methods (Hyman *et al*., 1992).

Paterson *et al.* (1992) used both steady-state and unsteady-state relative permeability measurements using Bowen Basin coal core samples. Using the steady state method, problems were encountered in the determination of saturation due to low porosity of coal and a long time was required to reach equilibrium. The JBN model was used to calculate relative permeability. As the relative permeability plots show, Paterson *et al.* (1992) could not obtain relative permeability data when water saturation was below 60%. They explained that these difficulties in data gathering were due to the small size of the core sample and the low absolute permeability. They also found that the low permeability of the samples was caused by mineralization in cleats. Paterson *et al.* (1992) stated that with acid leaching for instance hydrochloric acid, the permeability of their samples increased significantly. Figure 2.9 shows their relative permeability measurements.

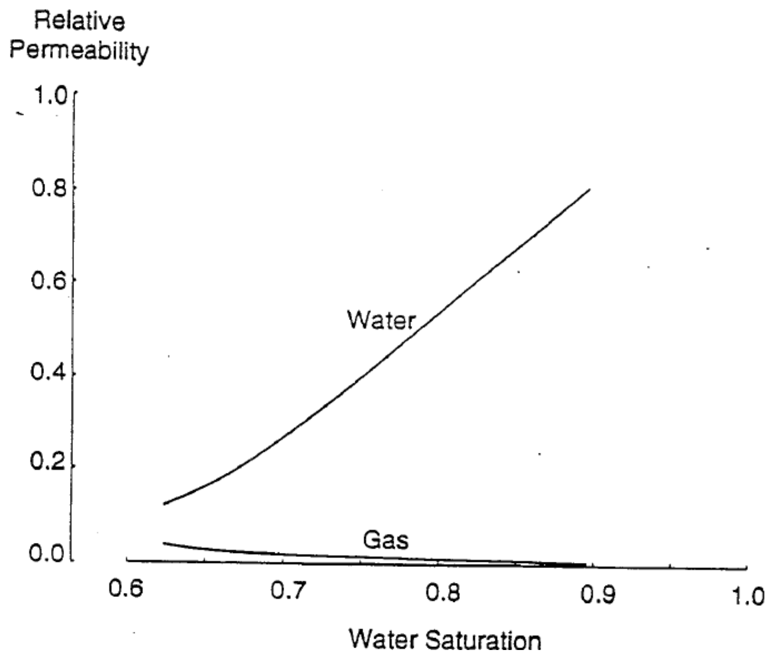

Figure 2.9 Relative permeability data for Bowen Basin coal core samples (Paterson *et al.*, 1992)

Dabbous *et al,* (1976) measured air/water drainage capillary pressure of coal samples using Pittsburgh and Pocahontas coals. They also studied the porosity of the coal samples to helium and water and the effect of overburden pressure on porosity. Helium porosity was determined with a helium porositimeter and water porosity was determined with the imbibition method. The porosity to gas was between 2.6 and 8.6% and the porosity to water was between 0.4 and 1.1 %. Results show that coal has different set of pore sizes; most of them are available to helium molecules but only larger pores are fracture are accessible to water. They obtained drainage capillary pressure data on the coal sample with 1½ inch diameter and capillary pressure between 7.4×10^3 and 2.54×10^6 dynes/ cm^2. The minimum irreducible water saturation that they can reach was 45%. Figure 2.10 shows the capillary pressure data versus corresponding saturation.

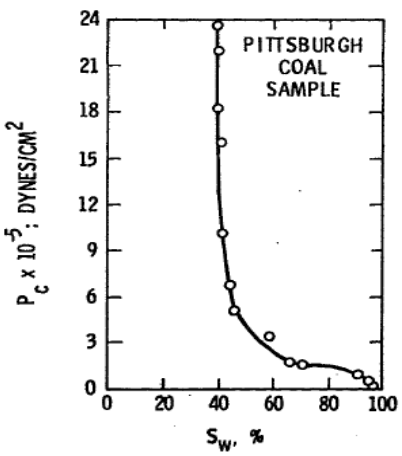

Figure 2.10 Capillary pressure data versus water saturation of Pocahontas coal samples (Dabbous et al., 1976)

Plug *et al.* (2008) compared the drainage and imbibition capillary pressure of four types of unconsolidated rock material in CO_2 /brine systems under reservoir conditions. The types of rock that they used were: fine grained sand, coarse grained sand, medium rank coal and high rank coal. They found the precision of the experiments by obtaining capillary pressure data for the four fine grained samples. The highest precision was ± 1.5 mbar. Figure 2.11 shows the capillary pressure data of the fine grained sand (160 < D < 210 μm).

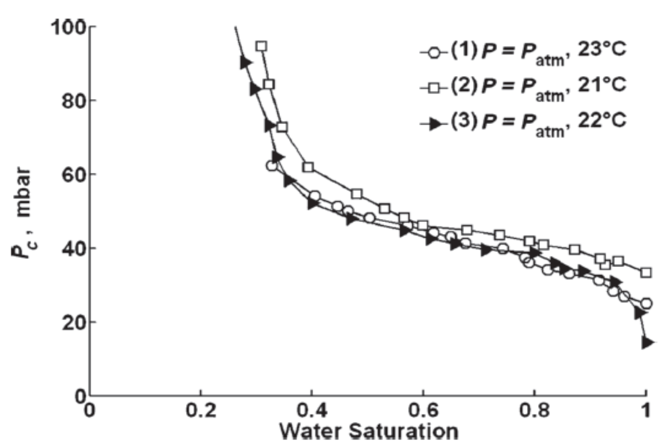

Figure 2.11 Drainage capillary pressure for CO_2 /brine systems at atmospheric conditions (Plug *et al.,* 2008)

Then they measured CO_2 and N_2 injections in coarse grained sand at various temperatures and pressures. Figure 2.12 shows the comparison of drainage capillary pressure for coarse- grained sand for CO_2 and N_2 injections.

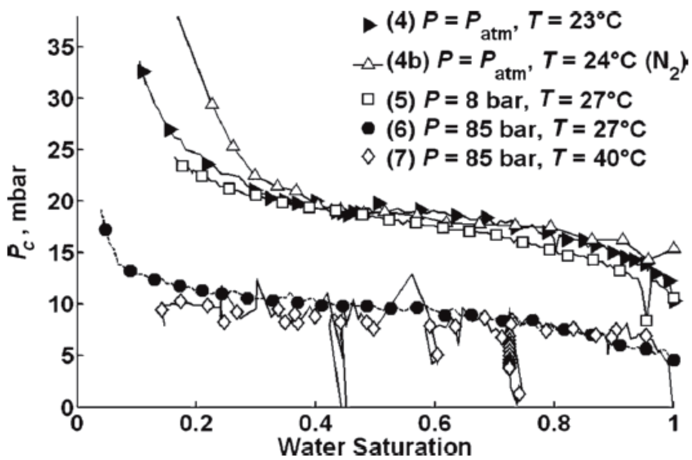

Figure 2.12 Drainage capillary pressure of coarse-grained sand (Plug et al., 2008)

With comparison of CO_2 and N_2 experiments 4 and 4b in the figure 2.12, it was observed that capillary pressure does not influence by the effect of CO_2 dissolution and it shows a same range for both N_2/water and CO_2/water systems.

The imbibition and drainage experiments using CO_2/ water systems in medium ranked coal show a good indication of a wettability effect. A decrease of the imbibition capillary pressure is observed for increasing CO_2 pressure which indicates the change in wettability from water wet ($P_c > 0$) to CO_2 wet ($P_c < 0$). Figure 2.13 shows the drainage and imbibition data for medium rank coal.

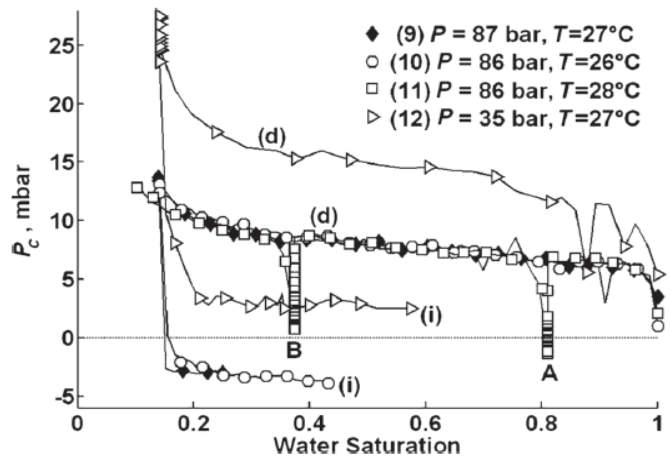

Figure 2.13 Drainage and imbibition capillary pressure data for medium coal sample (Plug *et al.,* 2008).

The last part of the Plug *et al*. (2008) experiments was the measurement of capillary pressure for high rank coal samples. Figure 2.14 shows the results of capillary pressure versus saturation for high ranked coal.

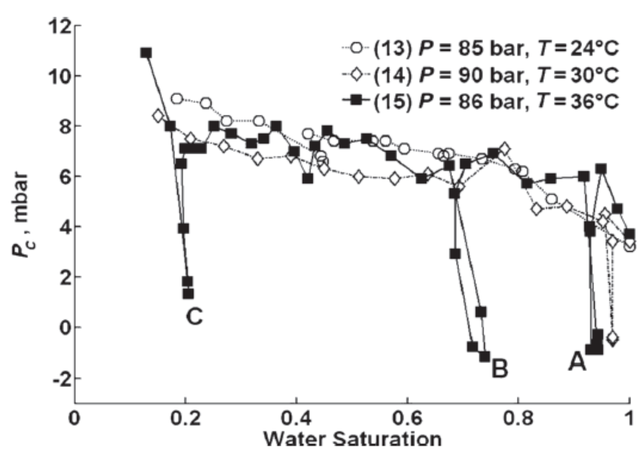

Figure 2.14 Drainage capillary pressure measurements for high ranked coal (Plug *et al*., 2008)

In contrast to medium ranked coal behaviour at high pressure, as it is shown in Fig. 2.14 , the P_c versus S_w curves for high ranked coal, show some irregularities especially in the temperatures near or higher than the critical CO_2 temperature.

2.13 SIMIULATION OF A COAL BED RESERVOIR

Numerical simulation of coal beds stared in the 1970s. These simulations were used to increase mine safety and prevent explosions with degasification (Price and Abdalla, 1972). Law *et al.* (2002) compared several simulators that have been used globally for coal bed reservoirs. They found that the recent simulators, which are more accurate consider natural facts and principals about fluid flow in coal. For instance, they account for the fact that coal has dual porosity and fluid flow is governed by Darcy's Law in cleats and by diffusion in its matrix, or the fact that the coal matrix shrinks during desorption. According to GRI (1996), a numerical simulator helps to obtain coal bed properties and improves production rates. Table 2.5 shows a summary of these simulators.

Table 2.5 Summary of Coal Bed Simulators (Law et al., 2002 and Wang et al., 2004)

Country	Source	Simulators
Australia	UNSW and CSIRO	SIMED
Canada	ARI and CMG	COMET EXODUS
UK	GeoQuest and Imperial college	ECLIPSE METSIMS
USA	BP and Penn State University	GCOMP

CHAPTER 3 EXPERIMENTAL PROCEDURE

3.1 SAMPLE COLLECTION AND PREPARATION

Coal chunk samples were provided by PIONEER Inc from the Prince Mine site in the Sydney Coal Field .These surface coal samples were extracted at depths of 15 to 150 ft. These samples were drilled parallel to the bedding, to make cores having a 1.5 diameter and 3 inch length. The procedure of drilling the coal samples was so hard and different methods were chosen to drill a perfect cylindrical coal core sample. To prevent breaking the cores during drilling, one idea was to place the coal chunk in concrete and let the concrete dry. Even though this attempt was not successful, three coal core samples were finally made and are shown in Fig. 3.1. The first plan was to use a core flood system (CFS), therefore two cores were coated with epoxy to obtain smooth cylindrical surface and also to prevent oxidation. However due to CFS break down, there was a change in the procedure of the thesis and capillary pressure equipment was used instead. Therefore, the coal core samples with epoxy cover were not suitable anymore. It was extremely time consuming and not practical for this experiment. Only one coal core sample was left for the experimental procedure.

a)

b)

Figure 3.1(a) Received coal chunks, (b) Drilled core samples

ASTM measurements were carried out at Dalhousie Mineral Engineering Center, to find the proximate analysis of the coal. Table 3.1 shows the proximate analysis of coal core samples from the Prince Mine, Sydney Coal field.

Table 3.1 Proximate Analysis of Coal Sample

Sample	Moisture (Wt. %)	Ash (Wt. %)	Volatile (Wt. %)	Fixed carbon(by difference) (Wt. %)	Sulfur(total) (Wt. %)	kJ/kg
1	3.02	7.22	55.8	34.0	2.49	30470
2	3.02	7.27	57.3	32.4	2.47	30017

3.2 PETRO PHYSICAL PROPERTIES OF COAL SAMPLE

3.2.1 BULK VOLUME DETERMINATION

Bulk volume can be calculated with either direct measurement or Archimedes measurement. Direct measurement is used for a cylindrical shape by measuring the length and diameter. Archimedes measurement can be used when the core sample does not have a perfect cylinder shape with a smooth and integrated surface.

3.2.2 PORE VOLUME MEASURMENT

To determine the pore volume, the initial dry core sample was weighed. Then the core sample was saturated with brine in a vacuum oven for 48 hours and weighed again. Pore volume was determined from:

$$P_v = \frac{M_w - M_d}{\rho} \tag{3.1}$$

Where

M_w = Wet weight [g]

M_d = Dry weight [g]

ρ = Density of brine [g/cm^3]

3.2.3 COAL CLEAT POROSITY MEASURMENT

The porosity of coal core sample to brine was determined by using gravimetric method. Coal porosity to brine was calculated from:

$$\Phi = \left(\frac{P_v}{p_b}\right) \tag{3.2}$$

where

Φ = Porosity

P_v = Pore volume [cm^3]

P_b= Bulk volume [cm^3]

According to Seidle.(2011) cleat compressibility is analogous to pore compressibility. Therefore, cleat porosity at reservoir condition is obtained by substituting cleat porosity at laboratory condition to the below equation.

$$\frac{\Phi}{\Phi_i} = \exp\left[- C_f (P_i - P)\right] \tag{3.3}$$

Where,

Φ = porosity at reservoir condition

Φ_i = porosity at laboratory condition

C_f= pore compressibility (psi^{-1})

P_i = laboratory pressure (psi)

P = reservoir pressure (psi)

3.3 BRINE COMPOSITION

The aim of this research is the determination of some petro physical characteristics of the Sydney Coal Basin at reservoir and laboratory conditions. The depth of the reservoir is assumed to be at 1000 m, therefore, brine should have the same composition as at the corresponding depth in the Sydney coal field. Martel *et al*. (2001) have done a thorough research about the composition of brine in the Sydney Coal Field. Based on their experiments, brine was made with the composition shown in the Table 3.2:

Table 3.2 Geochemical Composition of the Model Brine

Composition	Na	Ca	Mg	SO_4	Ba
mg/l	2650	345	93	0.02	177

3.4 EXPERIMENTAL SET UP

3.4.1 GRAVIMETRIC CAPILLARY PRESSURE SYSTEM (TGC-764)

The Gravimetric Capillary Pressure Unit is a device that provides capillary pressure measurements for liquid-gas systems. The Gravimetric Capillary Pressure Unit has a pressure control module and a humidifier unit. The pressure control module makes it possible to precisely control the desaturation pressure in the core sample. The humidifier humidifies the desaturation gas before it enters the porous medium to minimize the evaporation of pore water and to avoid saturation change that could be due to water vapor going into gas phase from the porous medium. Figure 3.2 shows the Gravimetric Capillary Pressure Unit (TGC-764).

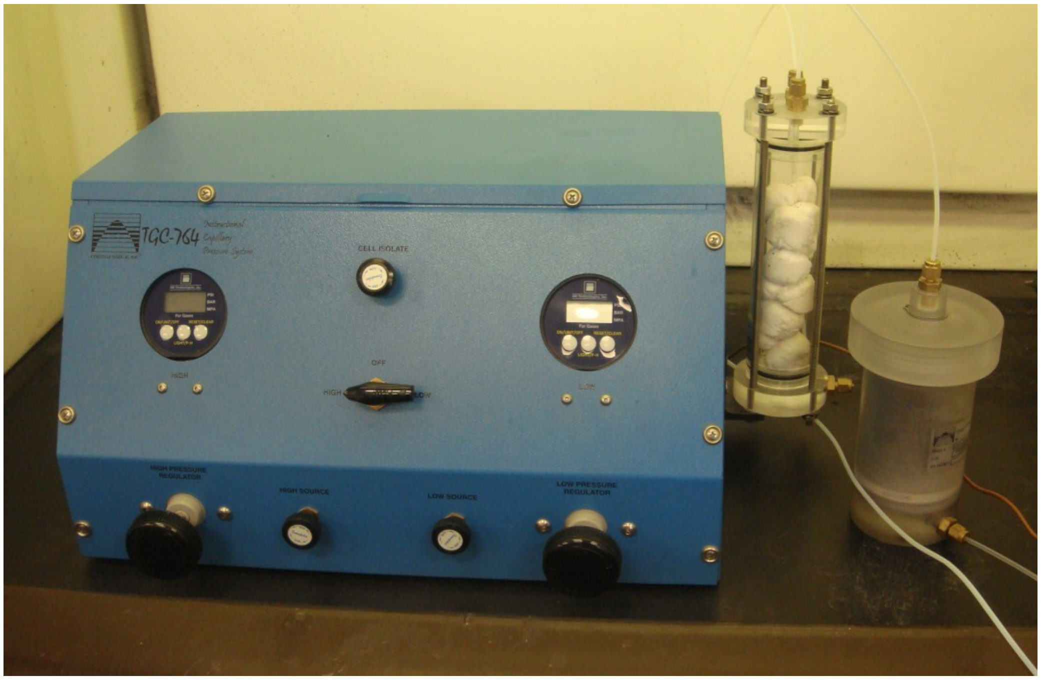

Figure 3.2 Gravimetric Capillary Pressure Unit (TGC-764)

The core holder consists of a ceramic plate, tissue and a spacer. The gravimetric capillary pressure unit (TGC-764) comes with different ceramic plates (1 bar, 3 bar and a 15 bar plates). The bar ratings of these plates refer to the expected threshold pressure of the plate. The 1 bar plates are for high permeability samples above 500 milidarcies, 3 bar plates are for samples with a permeability between 50 and 500 milidarcies and 15 bar ceramic plates are for less permeable samples. Ceramic plates should be saturated with brine in a vacuum oven for 24 hours before testing. The pressure regulator on the high pressure CO_2 cylinder should be set to 200 psi to avoid any damage to the equipment. A schematic of the Gravimetric Capillary Pressure Unit (TGC-760) is illustrated below.

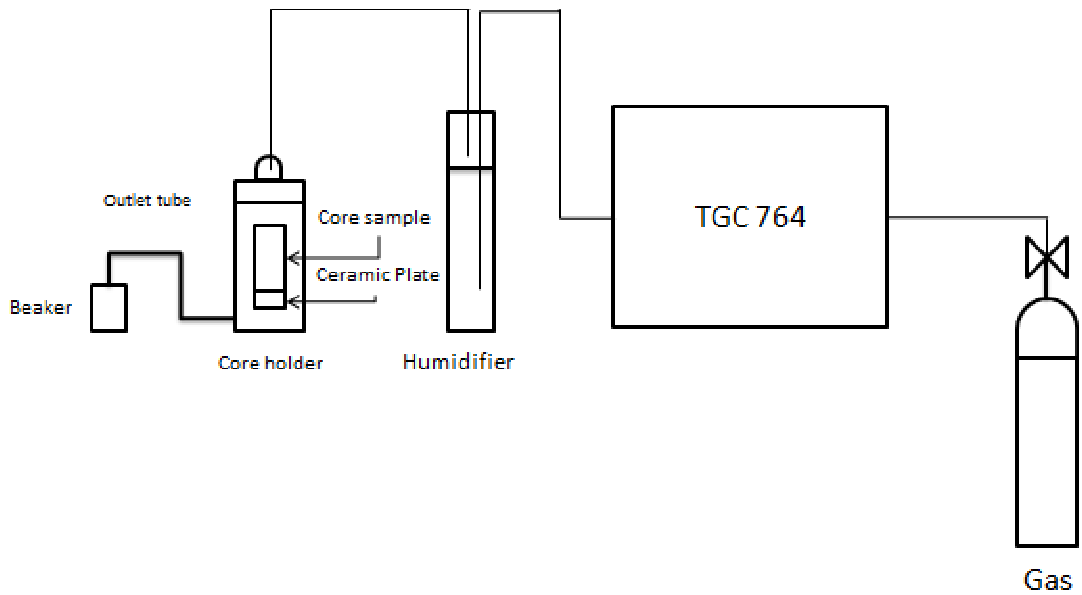

Figure 3.3 Schematic of measuring capillary pressure with TGC-764

To calculate the initial saturation of the sample, a 100% saturated sample is weighed and the water saturation is calculated from Eq.3.4:

$$\text{Saturation \%} = \left[\frac{\text{Saturated weight- Dry weight}}{\text{Pore Volume}}\right]\times 100 \qquad (3.4)$$

Once the initial saturation is determined the test can proceed. The saturated ceramic plate is placed inside the core holder, and then a piece of tissue with the same diameter as the core sample is placed on the ceramic plate. The saturated core sample is placed on top of the tissue on the ceramic plate. The pressure inlet valve to the cell is closed. The pressure is set to the desired initial pressure and the gas to the cell valve is opened. Normally a set of five pressures is used. Any suite of pressures may be used depending on the permeability of the core sample. With the gas to the cell valve opened, the displaced water/ brine is collected in a beaker from the outlet of the cell. This change in volume is recorded. When the volume in the does not change over an eight hour period, the volume should be read and the initial volume can be subtracted to obtain the displacement from the core samples and calculate water saturation at that specific pressure. Then the procedure is repeated for each of the pressure settings.

3.4.2 EXPERIMENTAL PREPARATION TEST

A preliminary test was conducted to test the equipment by measuring the capillary pressure data of well-known sandstone from Fontainbleau. Then the log-log graph of capillary pressure data versus saturation was plotted and the pore size distribution index was determined according to the Brook and Corey theory (1964). The results were compared with a published work of Oren et al. (1998). With the preliminary validation of the capability of the gravimetric capillary pressure system, the actual capillary pressure measurements for this research on coal core sample were initiated.

3.4.3 CAPILLARY PRESSURE MEASUREMENT AND RELATIVE PERMEABILITY DETERMINATION

The Sydney coal samples were first 100% saturated with brine in a vacuum oven for 48 hours and then weighed. The ceramic plate was saturated with brine placed in the core holder and then the saturated core sample was placed on top of it. Then the gas was introduced in to the core holder. Two different sets of experiment were conducted: the first for CO_2/brine and the second for methane/brine. Each test for capillary pressure measurements was repeated twice.

Using the data for capillary pressure and water saturation, the effective saturation and pore size distribution index were determined based on the Brook and Corey Equation 2.16. Then by substituting these data in Equation 2.18, the relative permeability was determined for CO_2/ brine and methane/brine systems.

3.4.4 CAPILLARY PRESSURE AT RESERVOIR CONDITION

To obtain the capillary pressure at reservoir condition, below Equations are used:

$$P_{c(Lab)} = \frac{(2\gamma \cos\theta)_{Lab}}{r_{Lab}} \tag{3.5}$$

$$P_{c(Reservoir)} = \frac{(2\gamma \cos\theta)_{Reservoir}}{r_{Reservoir}} \tag{3.6}$$

where

$P_{c(Lab)}$= Capillary pressure at laboratory condition [kPa].

$P_{c(Reservoir)}$ = Capillary pressure at reservoir condition [kPa].

γ_{Lab} = Interfacial tension at laboratory condition [N×10^3/m].

$\gamma_{Reservoir}$ = Interfacial tension at reservoir condition [N×10^3/m].

r_{Lab} = Pore radius at laboratory condition [m].

$r_{Reservoir}$ = Pore radius at reservoir condition [m].

$\cos\theta$ = Contact angle.

By dividing Eq. 3.5 by Eq. 3.6:

$$\frac{P_{c(Reservoir)}}{P_{c(Lab)}} = \frac{(\gamma \cos\theta)_{Reservoir}}{r_{Reservoir}} \times \frac{r_{Lab}}{(\gamma \cos\theta)_{Lab}} \tag{3.7}$$

It was recognized by Dabbous *et al.* (1976), It can be assumed that the cosine of the contact angle is 1 in the calculations for both laboratory and reservoir conditions. Therefore, Eq. 3.7 becomes:

$$P_{c(Reservoir)} = P_{c(Lab)} \frac{\gamma_{Reservoir}}{\gamma_{Lab}} \times \frac{r_{Lab}}{r_{Reservoir}} \tag{3.8}$$

The pore size distribution depends on the stress state of the porous medium. Under laboratory conditions the radius of a pore should be different from that under reservoir conditions. In this regard, the radius of the pore under laboratory condition can be related to the radius of the pore under reservoir condition using the definition of isothermal compressibility. We assume that the compressibility of a pore will be independent of temperature considering the depth of coal seam for this study. The isothermal compressibility definition is given by:

$$C_p = \frac{-1}{r_{Lab}} \frac{dr_{Lab}}{dP} \tag{3.9}$$

where

C_p = Pore compressibility [psi^{-1}].

r_{Lab} = Radius of pore at laboratory condition [m].

dr_{lab} = Change in the pore radius due to the overburden pressure changes [m].

dP = Overburden pressure changes [psi].

From Eq. 3.9:

$$C_p \times r_{Lab}\, \partial P = \partial r_{Lab} \tag{3.10}$$

Now, the radius of a pore under reservoir conditions is given by:

$$r_{Reservoir} = r_{Lab} - C_p \times r_{Lab}\, \partial P \tag{3.11}$$

$$r_{Reservoir} = r_{Lab}(\, 1 - C_p \times\, \partial P) \tag{3.12}$$

Substituting for r_{Lab}, from Eq. 3.12 into Eq. 3.8:

$$P_{c(Reservoir)} = P_{c(Lab)} \frac{\gamma_{Reservoir}}{\gamma_{Lab}} \times \frac{r_{Lab}}{r_{Lab}(\, 1 - Cp * dP)} \tag{3.13}$$

In Eq. 3.13, the denominator contains the compressibility of the coal and overburden pressure changes. According to Harpalani (1999), the pore compressibility of coal is 4.5 $\times 10^{-5}$ psi^{-1}. Dabbous *et al* (1976) Found that this amount in coal is constant for pressure above 1500 psi. The changes in the overburden pressure for the coal seam using in this research, which is at a depth of 1000 m, will give a pressure change of 3280 psi for an overburden pressure gradient of 1 psi/ft (Bradley *et al.,* 1989). According to Bennion.B. (2006) Equation 3.13 is applicable for determination of coal samples capillary pressure at reservoir condition from laboratory capillary pressure. The saturation measurements at laboratory condition can be correlated to the reservoir condition according to Section 2.7.9. Interfacial tension is a thermo-physical property with a negative temperature coefficient. Therefore, it is necessary to find interfacial tension of CO_2/ Brine systems at laboratory and reservoir condition. According to Chalbouad *et al.* (2006), the interfacial tension of CO_2/brine at reservoir conditions is approximately 27 mN/m and the interfacial tension at laboratory condition is approximately 73 mN/m and According to Firoozabady and Ramey (1988), these values for methane/brine system are approximately 49 mN/m and at laboratory condition are approximately 71 mN/m. Based on Eq.3.15, laboratory data for capillary pressure will be calculated for reservoir conditions.

3.4.5 PORE SIZE DISTRIBUTION

The last step of the experimental procedure was to determine the pore size distribution for both CO_2/brine and methane/brine systems. By substituting the capillary pressure data into Eq. 2.23, the largest pore throat was determined. Then ds/dp was determined using the least square fit. Using Burdin's theory, which was mentioned in Section 2.7.10, the pore size distribution was determined.

CHAPTER 4 RESULTS AND DISCUSSION

4.1 PETRO PHYSICAL PROPERTIES OF COAL SAMPLES

Bulk volume, pore volume and the porosity of the experimental coal samples were measured. Table 4.1 shows the results of these measurements.

Table 4.1 Porosity and Pore Volume Measurements of the Coal Sample

Bulk Volume	Archimedes Measurements : 85 cm^3
Pore volume	5.58 cm^3
Laboratory Cleat Porosity	0.065
Reservoir cleat porosity	0.056

The calculations for the figures in the Table 4.1 are shown in Appendix H

4.2 ANALYSIS OF COAL MICROSTRUCTURE

4.2.1 X-RAY DIFFRACTION (XRD)

XRD is a technique that provides information about the microstructure and chemical composition of materials without destroying them. To prepare coal for this experiment, the coal was ground and placed in the sample holder. Ǻ high-speed Bruker D8 Advance, using Cu-Ka radiation with a wave length of 1.54 Ǻ, tube voltage of 40 kV, and tube current of 40 mA, was used. In this technique the electrons accelerate toward the sample and the inner electrons gain energy for displacement. Therefore, they emit X-rays with different intensity. X-ray spectra are plotted, which shows the intensity of the reflected x-rays versus 2θ. θ is the angular position of detector which rotated around sample. In this experiment 2θ was set between 20° to 120°(Aminul and Farhat., 2009). In this research, XRD was used to analyze the chemical composition of a coal sample before they were used for the displacement test. Figure 4.1 shows the results of the XRD tests of Prince Mine coal samples.

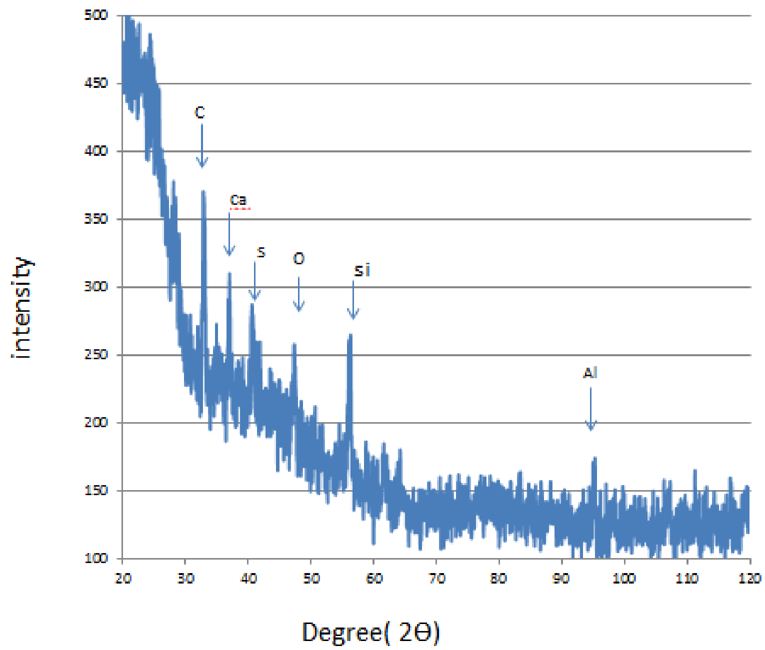

Figure 4.1 XRD results for Prince Coal Mine samples

XRD analysis shows that the most dominant elements in the coal sample are carbon, oxygen, silica, sulfur, aluminum and calcium. Existence of aluminum, oxygen, silica shows the existence of clay minerals.

4.2.2 SCANNING ELECTRON MICROSCOPY (SEM)

In scanning electron microscopy high-energy electrons interact with the atoms of the surface of the sample and generate signals that give information about the texture (morphology) and chemical composition of the sample. SEM can be used to magnify the surface up to 500,000 times and produce black and white, 2-D and 3-D images to determine the texture of materials. SEM has energy dispersion detector (EDS) that collects x-ray of different materials and show them into an energy spectrum. In this spectrum, each peak identifies a specific element and its concentration. For this purpose, two small pieces of coal with dimensions smaller than 1 cm^2 were cut and pasted on the holder and place in SEM equipment. Figure 4.2 shows the SEM images for different magnifications.

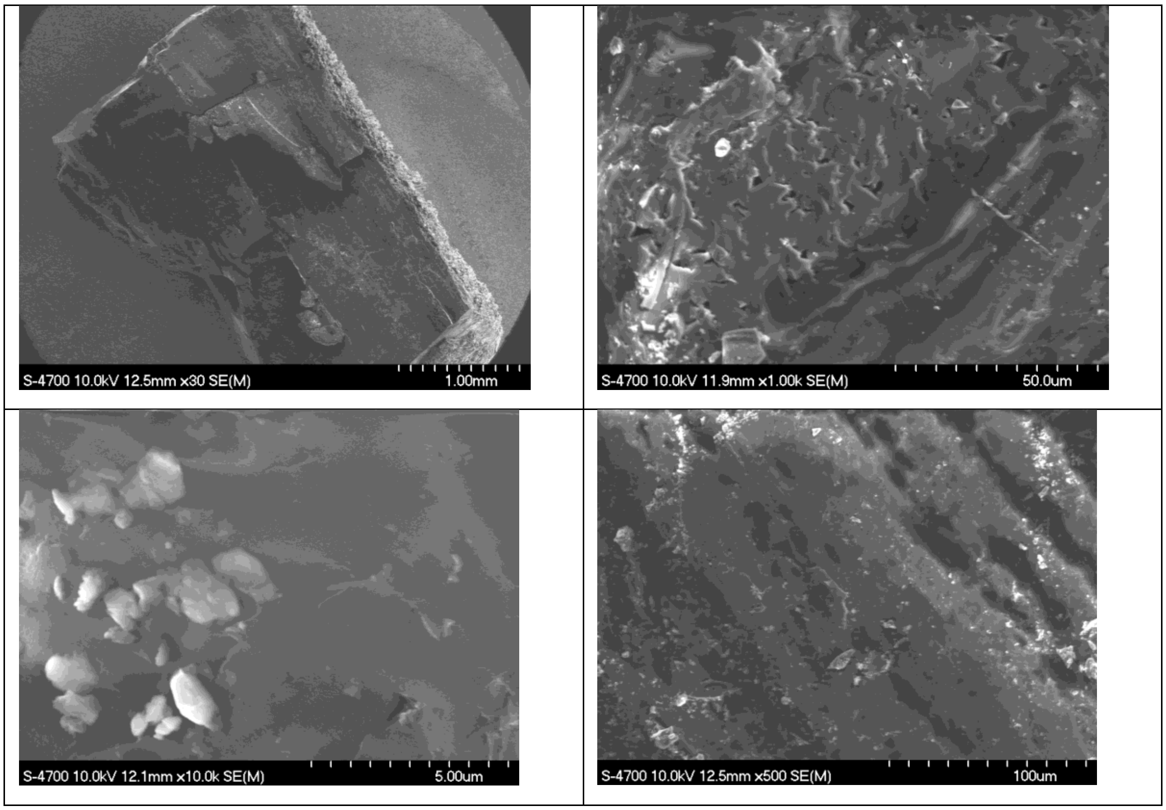

Figure 4.2 SEM analysis images at different magnifications of Prince coal mine.

Figure 4.3 shows the results of EDS and elemental analysis of the Prince Mine coal sample.

A

Element	Weight%	Atomic%
C	83.03	87.38
O	14.85	11.73
Al	0.36	0.17
Si	0.43	0.19
S	1.32	0.52

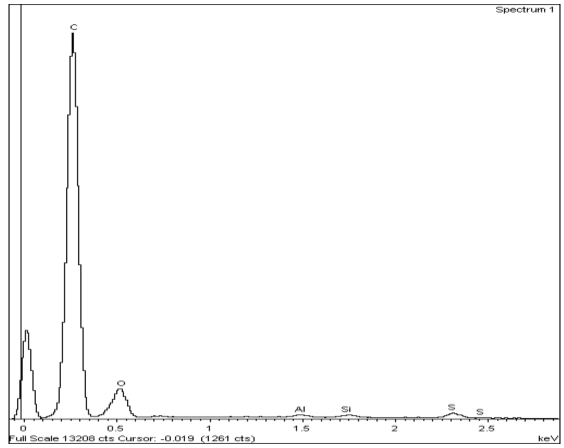

B

Element	Weight%	Atomic%
C	81.62	85.87
O	17.37	13.72
Al	0.13	0.06
Si	0.09	0.04
S	0.80	0.31

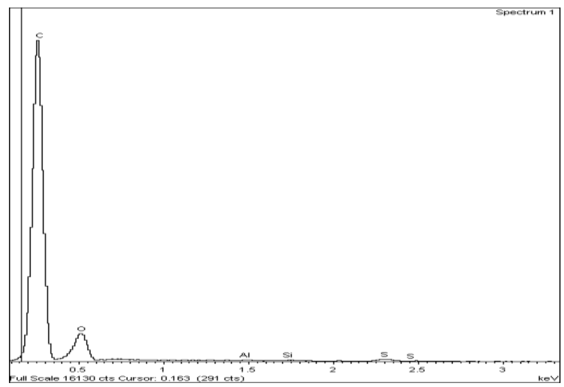

Figure 4.3 EDS and elemental analyses for Prince Coal Mine samples A and B

The results of SEM shows that the most dominant elements in coal are carbon, ocygen, aluminum , silica and sulfur, This analysis was carried out several times and the results are found in Appendix A.

4.3 BRINE CHARACTERIZATION

In this research, the brine had the same composition as that listed in Table 3.1. The details of density and viscosity measurements are described in the following sections.

4.3.1 BRINE DENSITY MEASUREMENT

According to ASTM D1429-08, the density of brine was determined by using a hydrometer (CAT.NO 2534). The hydrometer is a device for measuring liquid density and consists of a glass bulb weighted with mercury. Brine is poured in to the graduated cylinder and the hydrometer is lowered until it floats freely. This measurement was made at laboratory condition. The density of brine was found to be 1.021 g/cm$^{3.}$ The specific gravity may be corrected to 60/60°F by adding 0.0002 for each degree above 60°F. Therefore, the specific gravity may be expressed as:

Specific gravity = 1.021+ (77- 60)$\times$ 0.0002= 1.024 g/cm$^{3.}$

4.3.2 BRINE VISCOSITY MEASURMENTS

The viscosity of brine was measured with the Ubbelohde Viscometer at laboratory conditions. This device is a U shaped glass that uses capillary pressure principles for measuring viscosity. The viscosity of brine was measured as 1.10 cP.

4.4 PRELIMINARY TEST

The Fontainebleau sandstone core sample was saturated in a vacuum oven with distilled water. After 24 hours it was weighed, and the following are the gravimetric measurement details:

Core Dry Weight = 169.1 g

Core Saturated Weight = 176.6 g

Pore volume = $\frac{(176.6 - 169.1\ )}{1}$= 7.5 cm^3

By substituting the above data into Equation 3.6, the initial saturation of the Fontainebleau core sample is calculated as below:

Initial saturation = [(176.6 – 169.1) / 7.5]×100 = 100%

Then a saturated core sample was placed inside the core holder. CO_2 was made to displace the water. The displaced water was measured. By using the Brook and Corey equation the effective saturation for each capillary pressure was determined. Table 4.2 shows the capillary pressure and water saturation measurements of the Fontainebleau core sample.

Table 4.2 Capillary Pressure and Corresponding Saturation Measurements

S_w	S_e	LOG (S_e)	P_c	LOG (P_c)
1	1.00	0	0.2	-0.70
0.51	0.35	-0.46	2.3	0.36
0.42	0.23	-0.64	4	0.60
0.36	0.15	-0.83	9	0.95
0.28	0.04	-1.40	21	1.32
0.26	0.01	-1.88	40	1.60
0.25	0.00	-	45	1.65

Using the Brook and Corey theory, a log-log diagram of effective saturation and capillary pressure is a linear when the data for water saturation above 0.85 is omitted, as shown in Fig 4.4.

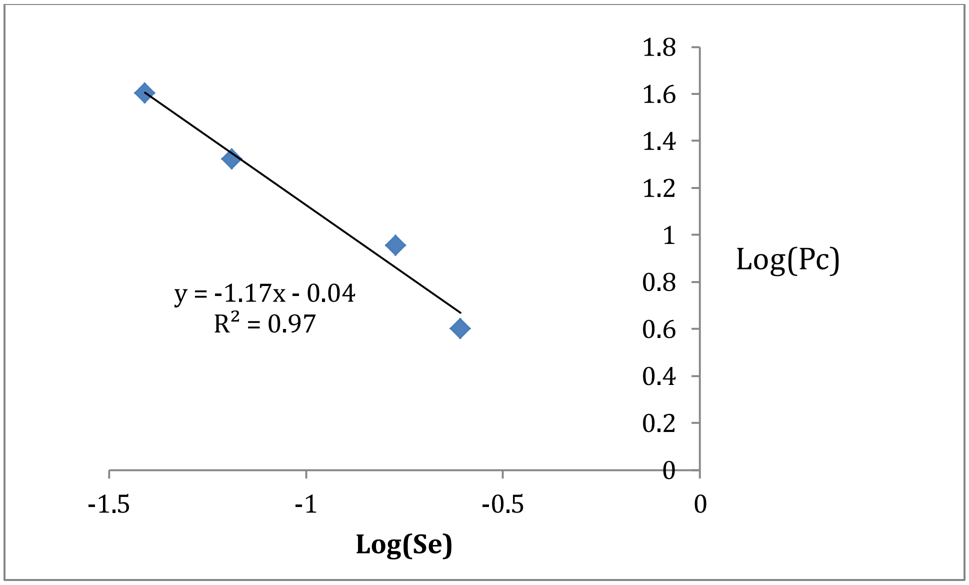

Figure 4.4 Log (P_c) vs. Log (S_e) for the Fontainebleau sample

The slope of the plot is given by the reciprocal of the pore distribution index $\frac{1}{\lambda}$. Therefore, the pore size distribution index is 0.85. Oren *et al*. (1998) examined capillary pressure as a function of saturation of Fontainebleau samples has been studied. Table 4.3 shows their data:

Table 4.3 Saturation Corresponding to Each Capillary Pressure (Oren et al., 1998)

S_w	S_e	log (S_e)	P_c	log (P_c)
0.34	0.18	-0.74	2.1	0.32
0.23	0.07	-1.15	4.7	0.67
0.21	0.05	-1.34	11.4	1.06
0.172	0.02	-1.85	33.5	1.52
0.167	0.01	-2.00	75.3	1.88
0.162	0.005	-2.30	145.2	2.16

The plot of log (S_e) versus log (P_c) is shown in Fig. 4.5:

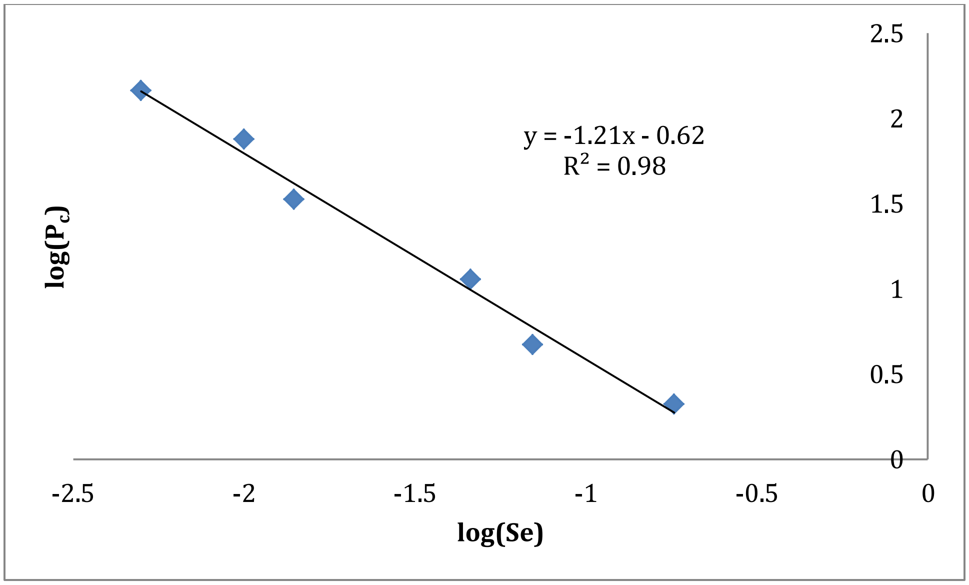

Figure 4.5 Diagram of log (P_c) versus log (Se) (Oren *et al.* 1998)

According to Oren *et al* (1998) the slope of the plot is the reciprocal of the pore distribution index ($\frac{1}{\lambda}$), which is 0.83. This is in good agreement with our laboratory findings for the pore distribution index, which was 0.85. By comparing the laboratory result with that of Oren *et al*. (1998), the error was 2.35% which is acceptable and enables us to carry out the actual experiment.

4.5 CAPILLARY PRESSURE MEASUREMENTS

To measure the relative permeability of Sydney coal samples, two different sets of experiments were conducted: the first for CO_2/brine systems and the second was for methane/brine systems. Each test for capillary pressure was repeated once.

4.5.1 CO_2/ BRINE SYSTEMS

After placing the saturated ceramic plate and core sample in the core holder, a high pressure source of CO_2 was connected to the gravimetric capillary pressure system (TGC-764). The pressure regulator was set to 200 psi for the input pressure of the TGC-764. . Table 4.4 shows the results of the capillary pressure versus saturation for the Prince coal sample for a CO_2/brine system.

Table 4.4 Capillary Pressure versus Saturation at Laboratory Conditions

P (psi)	P_c	S_w	S_e	Log(S_e)	Log (P_c)
14.9	0.2	0.98	0.95	-0.02	0.70
16	1.3	0.95	0.88	-0.05	0.11
20	5.3	0.87	0.70	-0.16	0.72
25	10.3	0.69	0.28	-0.55	1.01
30	15.3	0.63	0.14	-0.85	1.18
36	21.3	0.59	0.05	-1.33	1.33
42	27.3	0.58	0.02	-1.63	1.44
46	31.3	0.57	0.00	-	1.49

Using the obtained data, Figure 4.6 was constructed. It shows the drainage capillary pressure data versus corresponding saturations.

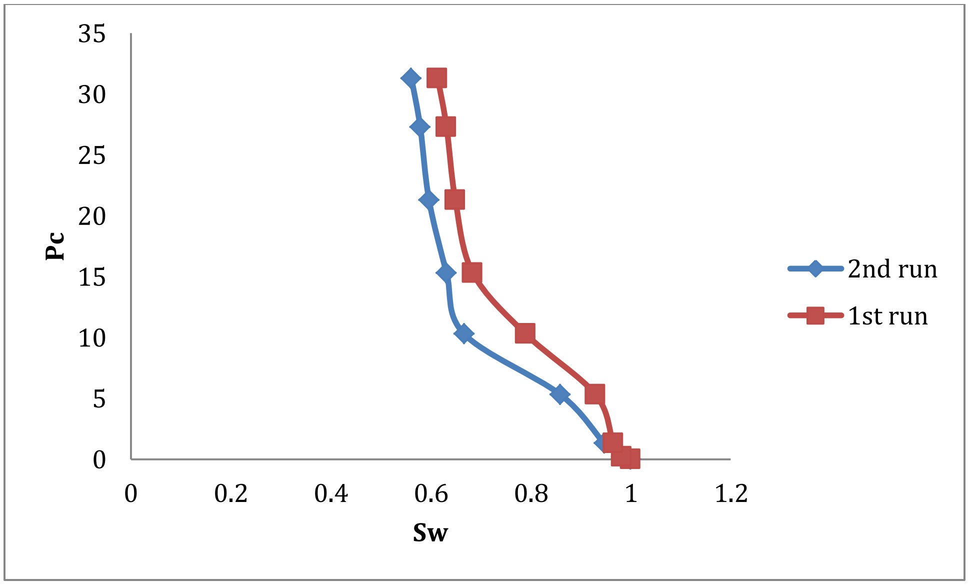

Figure 4.6 Drainage capillary pressure versus saturation

The next step was the determination of the pore size distribution index. Figure 4.7 shows a log-log plot of capillary pressure versus water saturation.

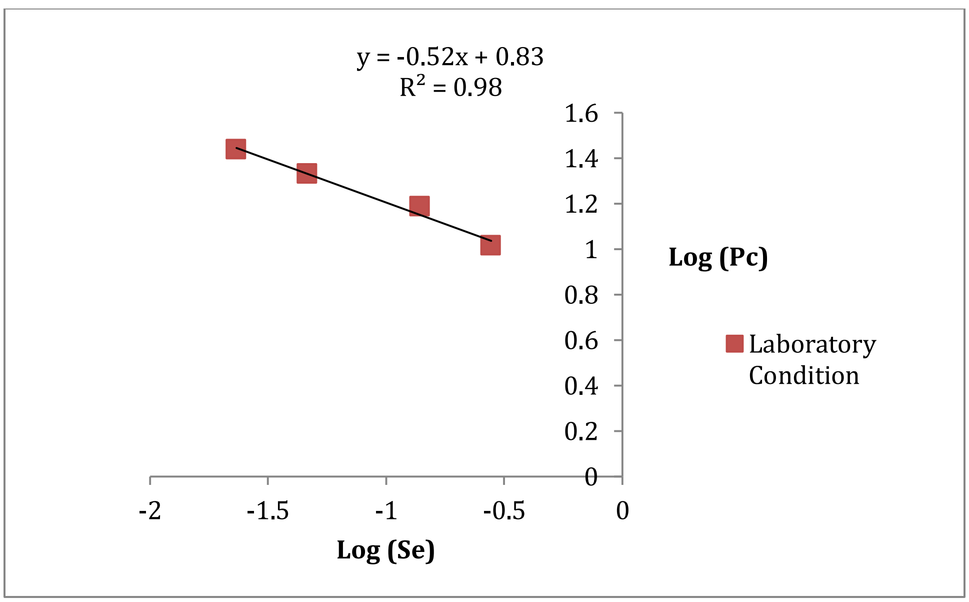

Figure 4.7 Log (Se) vs. log (Pc) for drainage capillary pressure

From the plot, the slope is -0.52. Therefore, $\lambda = 1/0.52 = 1.9$

Data for the second set of drainage capillary pressure data is shown in Appendix B.

4.5.2 CO_2/BRINE RELATIVE PERMEABILITY AT LABORATORY CONDITIONS

To calculate the relative permeability of CO_2/brine at laboratory conditions from the capillary pressure data, the Brook and Corey (1996) Equations 2.20 was used. Table 4.5 shows these results:

Table 4.5 Relative Permeability Measurements of CO2/ Brine

P_c	S_e	K_{rw}	K_{nrw}
0.2	0.95	0.812	0
1.3	0.88	0.596	0.003
5.3	0.70	0.236	0.045
10.3	0.28	0.006	0.475
15.3	0.14	0.001	0.724
21.3	0.05	0	0.899
27.3	0.02	0	0.959

Figure 4.8 shows the relative permeability of CO_2/brine versus saturation

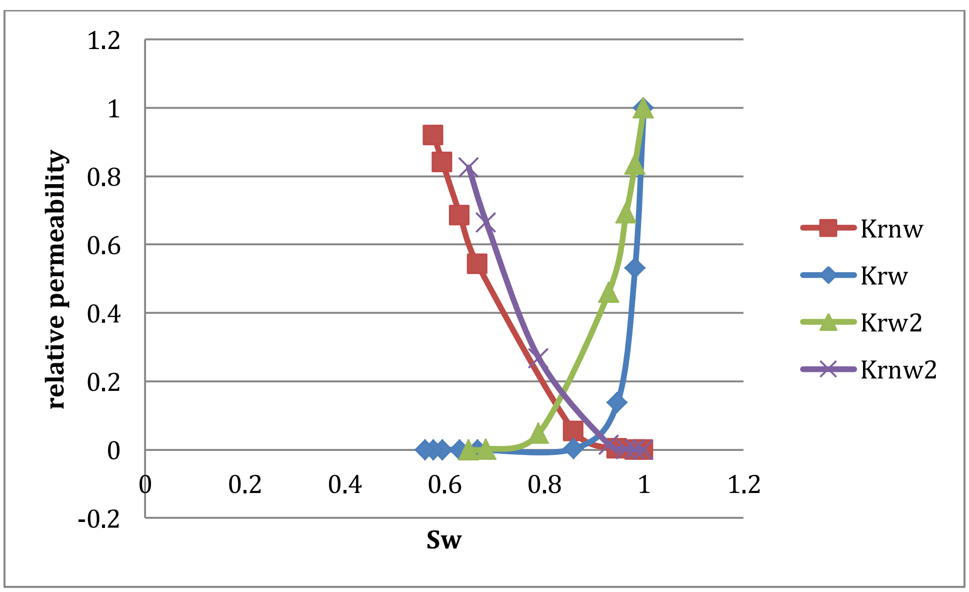

Figure 4.8 Relative permeability of CO2/brine system at laboratory conditions

4.5.3 CO2/ BRINE CAPILLARY PRESSURE AT RESERVOIR CONDITION

To obtain the capillary pressure at reservoir conditions, Equation 3.13 is used:

$$P_{c(Reservoir)} = \frac{P_{C(lab)} \times (\gamma \cos\theta)_{Reservoir}}{(\gamma \cos\theta)_{Lab}} \frac{1}{(1 - C_P dp)}$$

$$P_{c(Reservoir)} = \frac{P_{C(lab)} \times 27}{73} \frac{1}{(1 - 4.5\times10^{-5}\times(3280-14.7))} = 0.43\, P_{c(\text{lab})}$$

After substituting the capillary pressure measurements at laboratory condition in the above equation and also finding the brine saturation at reservoir condition, a log-log diagram of P_c and the effective saturation at reservoir condition were plotted. Figure 4.9 show the log-log plot of capillary pressure versus saturation at laboratory and reservoir conditions.

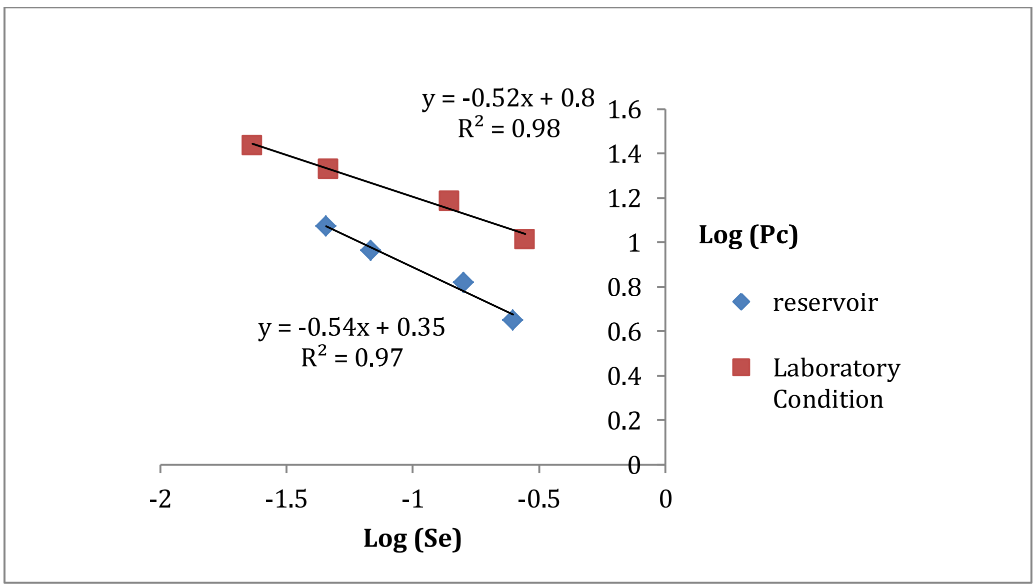

Figure 4.9 Comparisons of log-log capillary pressure data vs. saturation at laboratory and reservoir conditions

The slope at reservoir condition is (-0.54), therefore, λ= 1/0.54= 1.85

4.5.4 CO_2/BRINE RELATIVE PERMEABILITY RESERVOIR CONDITION

To calculate relative permeability of CO_2/brine at reservoir condition from the capillary pressure data, the Brook and Corey (1996) Equations 2.20 were used. Table 4.6 shows these results:

Table 4.6 Relative Permeability Measurements of CO2/brine

P_c	S_e	K_{rw}	K_{nrw}
0.08	0.95	0.827	0
0.56	0.88	0.612	0.003
2.29	0.68	0.210	0.053
4.45	0.25	0.003	0.524
6.61	0.16	0.001	0.687
9.20	0.07	0	0.863
11.79	0.04	0	0.909

Figure 4.10 shows the relative permeability of CO_2/brine versus saturation at reservoir condition.

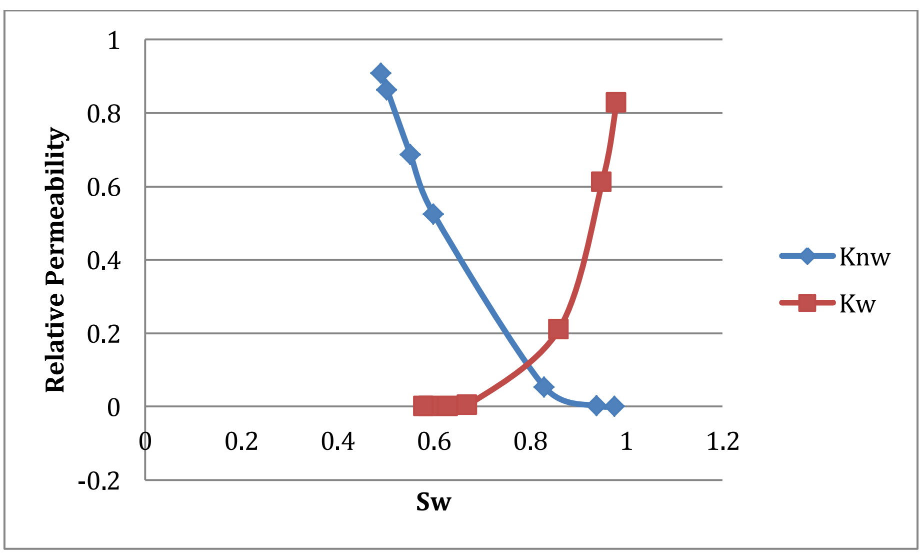

Figure 4.10 Relative permeability of CO2/brine system at reservoir condition

4.5.5 PORE SIZE DISTRIBUTION OF CO_2/BRINE SYSTEM

The pore size distribution can be obtained for CO_2/brine systems by using Eq.2.26. It was mentioned in section 3.4.4, that the interfacial tension of CO_2/brine is 73 (mN/m). According to Equation 2.26, to obtain pore size distribution ($D(r_i)$), it is necessary to calculate ds/dp. It was stated by Donaldson *et al.* (1991) that capillary pressure and saturation data are best fitted in a hyperbolic function. Therefore ds/dp could be found with a least square solution. To do so, procedure below was conducted; the detail of this calculation is outlined in Appendix D.

Table 4.7 Least Squares Calculation of $y(P_c)$ as a Function of $x(S_w)$ and Pore Size Distribution of CO_2/ Brine Drainage

$y(P_c)$	$x(S_w)$	x^2	xy	y^2	x^2y^2	r_i	$D(r_i)$
0.08	0.95	0.90	0.08	0.01	0.01	105.87	0
0.56	0.88	0.77	0.49	0.31	0.24	16.29	0.01
2.29	0.68	0.46	1.59	5.24	2.42	3.99	0.11
4.45	0.25	0.06	1.11	19.80	1.24	2.06	0.37
6.61	0.16	0.03	1.06	43.69	1.12	1.38	0.80
9.20	0.07	0.005	0.64	84.64	0.41	0.99	1.50
11.79	0.04	0.002	0.47	139.00	0.22	0.78	2.44

After calculating dS_w/dP with the least squares method by substituting the results in Equation 2.24, the pore size distribution was determined. Figure 4.11 shows the statistically calculated the pore size distribution versus pore radius.

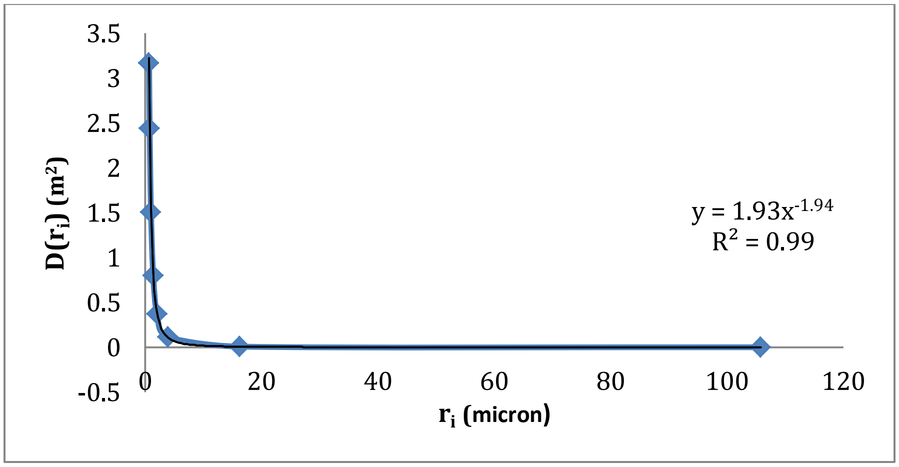

Figure 4.11 Pore size distribution for CO_2/brine drainage

As was expected from fractal theory, the pore size distribution should fit a power law function and the exponent shows the calculated pore size distribution index of 1.94

4.5.6 METHANE BRINE SYSTEMS

To measure the relative permeability of methane/brine systems, the same procedure as that for the CO_2/brine systems was repeated. Table 4.8 shows the data for capillary pressure obtained for methane/brine systems.

Table 4.8 Capillary Pressure Measurement at Laboratory Condition

P_c [psi]	S_w	S_e	Log(S_e)	Log (P_c)
0.3	0.98	0.94	-0.03	0.52
1.5	0.94	0.82	-0.09	0.18
5.3	0.90	0.67	-0.17	0.72
11.1	0.83	0.4	-0.40	1.04
15.3	0.73	0.13	-0.89	1.18
25.2	0.70	0.05	-1.30	1.40
27.6	0.69	0	-	1.44

From the obtained data, Fig. 4.12 shows the drainage capillary pressure plot versus corresponding saturation for methane/brine systems

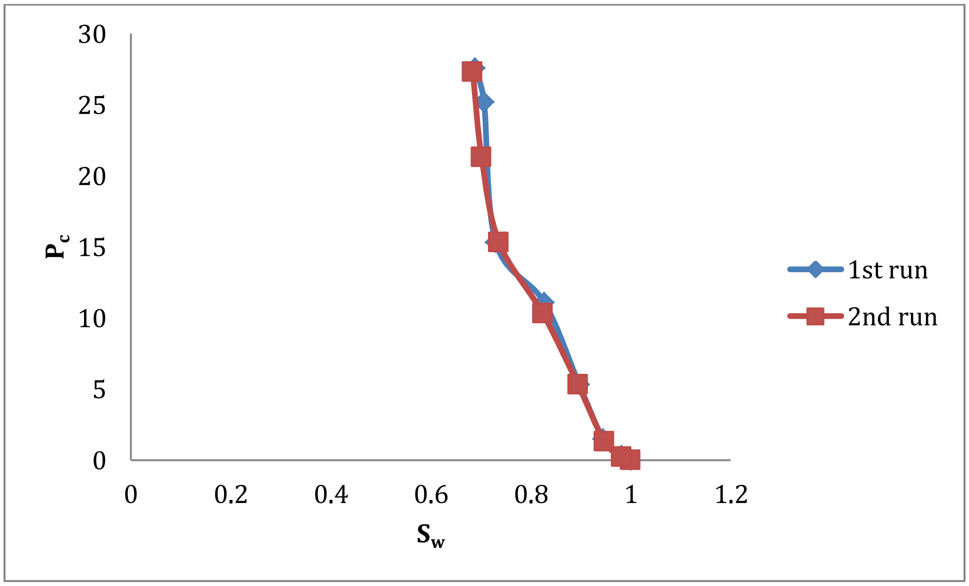

Figure 4.12 Drainage capillary pressure versus saturation for methane/brine systems

The next step in the determination of the pore size distribution index is a log-log plot of capillary pressure versus effective saturation, as shown in Fig.4.13

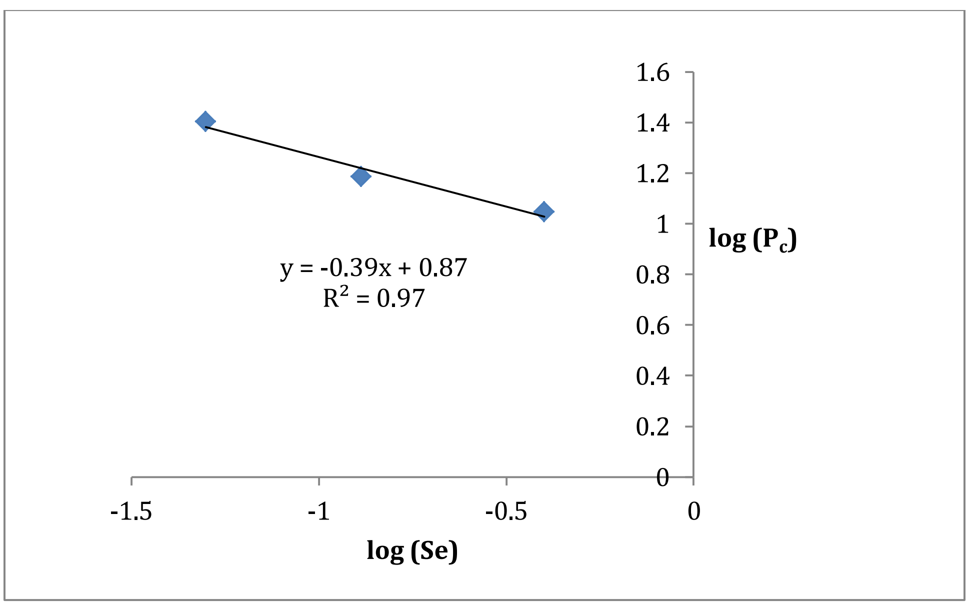

Figure 4.13 Log (S_e) vs. Log (P_c) for drainage capillary pressure

From the Brook and Corey theory, the slope is -0.39, therefore, $\lambda = 1/0.39 = 2.56$.

Data for the second set of measurements are in Appendix E.

4.5.7 METHANE/BRINE RELATIVE PERMEABILITY AT LABORATORY CONDITIONS

Relative permeability of methane/brine at laboratory conditions was calculated with the capillary pressure data (Brook and Corey, 1996). Table 4.9 shows these results:

Table 4.9 Relative Permeability Measurements of Methane/ Brine

P_c [psi]	S_w	S_e	K_{rw}	K_{nrw}
0	1	1	1	0
0.3	0.98	0.94	0.803	0.001
1.5	0.94	0.82	0.479	0.012
5.3	0.90	0.67	0.219	0.065
11.1	0.83	0.4	0.046	0.315
15.3	0.74	0.13	0.001	0.750
25.2	0.73	0.05	0	0.901
27.6	0.69	0	0	1

Figure 4.14 shows the relative permeability of methane/brine versus saturation :

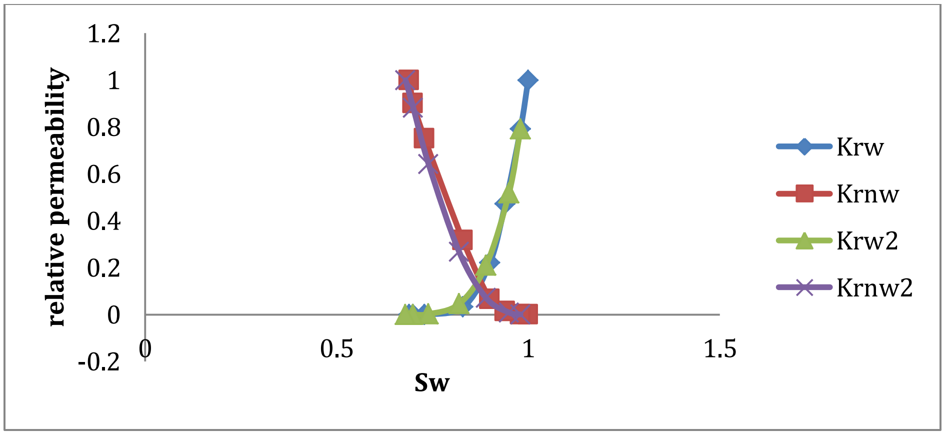

Figure 4.14 Relative permeability of methane/brine system at laboratory conditions

The relative permeability data for a second set of capillary pressure measurements are in Appendix F.

4.5.8 METHANE/BRINE CAPILLARY PRESSURE AT RESERVOIR CONDITIONS

To obtain the capillary pressure at reservoir conditions the same procedure as that for methane has been repeated. Figure 4.15 show the log-log plot of capillary pressure versus saturation at laboratory and reservoir condition.

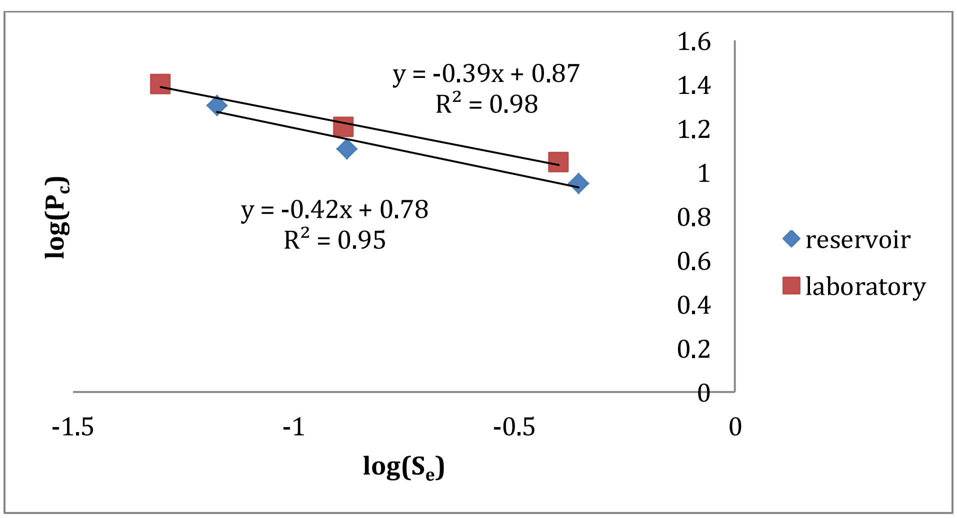

Figure 4.15 Comparisons of log-log capillary pressure data vs. saturation at laboratory and reservoir conditions

According to Brook and Corey theory (1996), the slope is (-0.42), therefore, $\lambda = 1/0.42 = 2.38$

4.5.9 METHANE/BRINE RELATIVE PERMEABILITY AT RESERVOIR CONDITION

Relative permeability of methane/brine at reservoir conditions was calculated based on Brook and Corey equations (1996), Table 4.10 shows these results:

Table 4.10 Relative Permeability Measurements of Methane/ Brine

P_c [psi]	S_w	S_e	K_{rw}	K_{nrw}
0	1	1	1	0
0.2	0.98	0.93	0.782	0.001
1.2	0.93	0.81	0.453	0.014
4.2	0.87	0.67	0.227	0.063
8.9	0.79	0.44	0.050	0.255
12.8	0.68	0.13	0.001	0.743
20.2	0.66	0.07	0	0.867

The figure 4.16 shows the relative permeability of methane/ brine versus saturation.

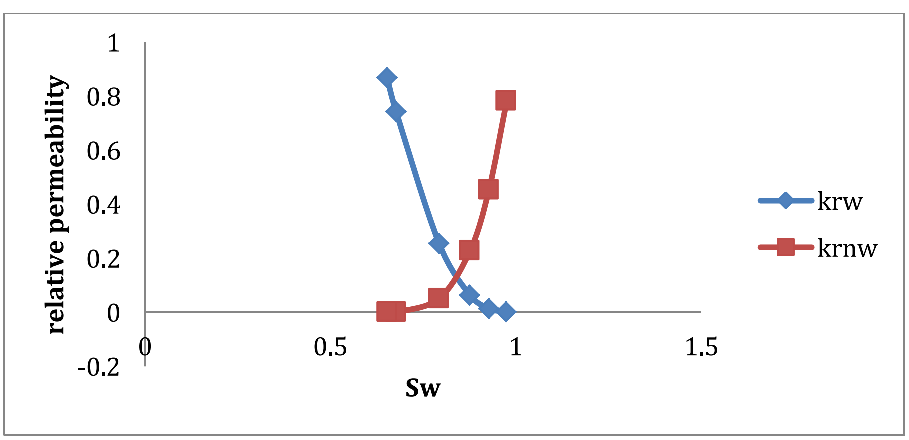

Figure 4.16 Relative permeability of a methane/brine system at reservoir conditions

4.5.10 PORE SIZE DISTRIBUTION OF METHANE/BRINE SYSTEM

Pore size distribution data for the of methane/brine system were obtained from the measured saturation and capillary pressure data. The same procedure as that for the CO_2/brine system was carried out. Again, the value of cos θ was assumed to be 1 in all test conditions.

By having capillary pressure and saturation data, with least squares calculation ds/dp can be found. Then the pore size distribution for each capillary pressure test was calculated for methane/brine systems.

Table 4.11 Pore Size Distribution Data from Methane/Brine Drainage

$y(P_c)$	$x(S_w)$	x^2	xy	y^2	x^2y^2	r_i	$D(r_i)$
0.2	0.98	0.96	0.24	0.06	0.06	70.58	0
1.2	0.93	0.86	1.12	1.44	1.25	14.17	0.003
4.2	0.87	0.76	3.69	17.98	13.61	3.99	0.009
8.9	0.79	0.62	7.04	78.85	49.21	1.91	0.012
12.8	0.67	0.45	8.58	163.84	73.55	1.38	0.554
20.2	0.66	0.44	13.31	406.43	177.04	0.84	2.144

With $D(r_i)$ and r_i which are shown in Table 4.11, a plot of pore size distribution for methane/brine was obtained.

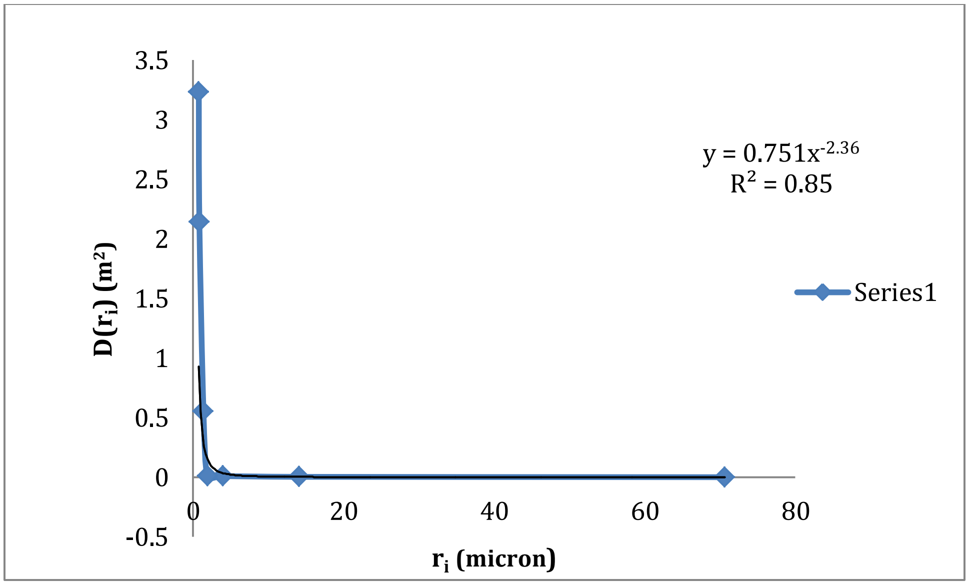

Figure 4.17 Pore size distribution for methane/brine drainage

As is shown in the Figure 4.17, the exponent of the fitted power law function shows the statistical pore size distribution index as 2.11.

Data of for the second drainage pore size distribution is shown in Appendix G.

4.6 DISCUSSION

X-Ray Diffraction analysis (XRD) of the powdered coal shows the intensities of various elements found in the coal samples. The dominant minerals are calcium, sulfur, silica, aluminum, oxygen and carbon. The peaks due to the aluminum, silica and oxygen are due to argillaceous or clay minerals. According to Mukhopadhyay *et al*., (1998) the minerals occur in coal from plants found in swampy regions. They fill coal pores and reduce permeability. Under swampy condition feldspars are chemically disintegrated into fledspartic mud. Since these are alumosilicates, the chemically distinguished products constitute clay minerals.

Scanning electron microscopy (SEM) shows that Prince coal is not highly porous. EDS and elemental analysis were also obtained to determine the elements and their intensity within the sample. It was observed in Fig 4.3 that the coal sample had large amounts of aluminum, silica, calcium carbonates and sulfur. According to Manoj et al., (2009) the light luminosity in Fig 4.2 shows the presence of aluminum and dark luminosity shows the presence of chalcophiles. These elements show the calcination of calcite or dolomite due to thermal shock which occurs during metamorphism process.

Gravimetric Capillary Pessure Unit was used to determine capillary pressure and saturation data for CO_2 / brine and methane/brine systems. By obtaining laboratory data for capillary pressure and saturation data the values under reservoir conditions were deduced based on the established relations in the petroleum industry.

The relative permeability and pore size distribution for both systems were determined from the experimental data. In the capillary pressure versus water saturation plots, it was observed that the methane/brine system had higher irreducible water saturation than the CO_2 /brine system. There are a number of factors that determine displacement efficiency, such as wettability, interfacial tension and viscosity ratio. The difference in irreducible water saturation for the two systems is due to difference in interfacial tension between CO_2 / brine and methane/ brine as well as the viscosity ratio.

Comparing Fig 4.6 and 4.12, two curves for the drainage experiment on the methane/brine system are closer together than in the CO_2 /brine system. A study by Kailas (2012) established a change in the wettability of Fontainebleau sandstone due to CO_2 injection. CO_2 interaction changes the wettability in way that results in less water wetted. This means that the surface of coal will be less water wetted and will result in a decrease in saturation.

In this work comparison of methane/brine and CO_2/brine relative permeability versus saturation plots shows that the curve for methane/brine is less concave. For a multiphase flow in the porous medium, the fractional flow of a given phase is the fraction of the total flow assigned to that phase at a given point. For higher efficient recovery the fractional flow of the resident fluid must be higher than that of the injected fluid. Now by comparison of the relative permeability of methane/brine and CO_2/brine at reservoir condition, it is observed that methane/brine has higher relative permeability than the CO_2/brine system. This means that the fractional flow of methane is higher and therefore this makes this flied a good candidate for CO_2 sequestration and enhanced coal bed methane production.

Comparing log-log plots of capillary pressure versus saturation at laboratory and reservoir conditions in Figure 4.9 and 4.16, the pore size distribution index at laboratory condition is larger than that at reservoir conditions. Generally the larger the pore size distribution index the less heterogeneous the reservoir rock is. This also means that the fractal dimension of the porous medium is small. Under reservoir condition the stress will collapse the larger pores resulting in more of the smaller pores than the larger pores. Therefore under reservoir condition the porous medium has a wider pore size distribution and the fractal dimension of the porous medium is big and the pore size distribution index is small. This explains the observations.

Fig 4.11 and 4.17 show plots of pore size distribution versus pore size for the coal samples. These figures provide statistical chances of finding particular pore sizes in the samples. It shows that the smaller pores have wider distributions than larger pores and this trend has also been reported for sedimentary rock samples (Tiab and Donaldson, 2004). These plots have been fitted with a power law approximation with a regression coefficient of 0.99 for a CO_2/brine system and 0.84 for a methane/brine system. The pore size distribution index for CO_2/brine is 1.917 ± 0.025 and for methane/brine is 2.439 ± 0.327. The interaction of CO_2 and coal will change the wettability and this will change the capillary pressure characteristic of the system. Pore size distribution is deduced from capillary pressure data and also the size of the gas molecules. Methane is tetrahedral and acts more as a sphere than CO_2, which is linear. This will allow CO_2 molecules to penetrate into smaller pores than CH_4 molecules. Therefore different pore size distribution indices are expected for the coal sample using different gases.

The theoretical reason for the choice of the power law approximation lies in the fact that pore sizes of porous samples have been found to exhibit fractal behavior. This means that they have a fractal dimension. This permits a power law relationship between the pore size and their distributions. It therefore stands to reason that since fluid saturation is associated with the pore space, when capillary pressure versus saturation data, when fitted with a hyperbolic model it will give a pore size distribution with a power law behaviour.

CHAPTER 5 CONCLUSION

Current trends in global warming are due to anthropogenic carbon dioxide presence in the atmosphere. Mitigating this trend will require the capture and storage of carbon dioxide in geologic repositories. Deep unmineable coal seams are targeted because of value added sequestration. The injection of CO_2 and the production of coal bed methane require adequate knowledge of the petro physical properties of the coal seam. In this study relative permeability, capillary pressure and the pore size distribution indices of the coal sample for Sydney Basin coal have been determined. The following are the conclusions:

1- Coal samples from Sydney Basin have been found from XRD and SEM analysis to contain clay minerals.
2- The SEM images show extensive micro pores and this is an indication of large gas storage capacity.
3- The pore size distribution plots show that the smallest pores are the most abundant and this agrees with pore size distribution plots for other geologic porous samples.
4- The relative permeability and capillary pressure plots obtained using the pore size distribution index and the empirical relative permeability equation from Brook and Corey (1996) show similar shapes and trends to those obtained from displacement experiments presented by other researchers using core flooding experiments.
5- The systematic approaches used in the laboratory experiments together with the sophistication of the equipment make these petro physical data an invaluable source of data for planning future enhanced coal bed methane production from the Sydney Coal Field.

The original plan was to use the sophisticated Core Flooding System (CFS-700) that offers an opportunity for reservoir condition testing. The breakdown of this equipment causes a change in laboratory planning with regard to experimentation. Therefore, the recommendation of this study is that these petro physical data should be generated under reservoir conditions using this system when it becomes functional.

REFERENCES

Ahmed T. (1946). *Reservoir Engineering Handbook.* Second Edition. TNB71. A337 2000.

Akinnikawe O., Chaudhary A., Vasquez O., Enih C., Ehlig-Economides C. A. (2010). *Increasing CO_2 – Storage Efficiency Through a CO_2 – Brine Displacement Approach*; SPE 139467.

Aminian K., (published year not given). *Coalbed Methane – Fundamental Concepts.* Petroleum & Natural Gas Engineering Department, West Virginia University: karl.nrcce.wvu.edu/regional/CoalbedMethane_Aminian_Paper_1.pdf

Aminian K., (published year not given). *Evaluation of Coalbed Methane Reservoirs.* Petroleum & Natural Gas Engineering Department, West Virginia University: karl.nrcce.wvu.edu/regional/CoalbedMethane_Aminian_Paper_2.pdf

Aminul .MD and Farhat.Z, (2009) *.Wear of A380M Aluminum Alloy Under Reciprocating Load.* Journal of Materials Engineering and Performance. Vol.19.

Anderson J., Simpson M., Basinski P., Beaton A., Boyer C., Bulat D., Ray S., Reinheimer D., Schlacter G., Colson L., Olsen D., John Z., Khan R., Low N., Ryan B., and Schoderbek D.(2003). *Producing Natural Gas from Coal*. Oilfield Review, pp. 8-30.

Beaton A., Lagenberg W., and Pana C. (2006). *Coalbed Methane Resources and Reservoir Characteristics from the Alberta Plains, Canada*. International Journal of Coal Geology, Vol. 65, pp. 93–113.

Bennion D. B. and Bachu, S. (2006). *Supercritical CO_2 and H_2S – Brine Drainage and Imbibition Relative Permeability Relationships for Intergranular Sandstone and Carbonate Formations*. SPE 99326.

Bradley .D.A., Chia .Y.(1989). *Evaluation of Reservoir Compaction and Its Effects on Casing Behavior.* SPE Production Engineering. Vol. 4, No. 2.

Brook R.H and Corey A.T (1996). *Hydraulic Properties of Porous Media*. Colorado state university hydrology paper, Fort Collins.Vol 27.

Buckley S.E., and Leverett M. C. (1942). *Mechanism of Fluid Displacement in Sands*. Transactions of AIME, Vol. 146, pp. 107-116.

Burdin.N.T.,Gourney.L.S and Reichertz.P.P. (1950). *Pore Size Distribution of Petroleum Reservoir Rocks*. Trans.AIME.Vol. 198. pp. 195-204.

CCST @ MIT; "http://sequestration.mit.edu/tools/projects/storage_only.html" (Accessed 13th August, 2011).

Chalbouad.C., Robin.M., Egermann.P.(2006). *Interfacial Tension Data and Correlation of Brine/CO_2 Systems Under Reservoir Condition.* SPE 102918.

Cheung K., Sanei H., Klassen P., Mayer B., and Goodarzi F. (2009). *Produced Fluids and Shallow Groundwater in Coalbed Methane (CBM) Producing Regions of Alberta, Canada*: *Trace Element and Rare Earth Element Geochemistry*. International Journal of Coal Geology,Vol.77, pp. 338–349.

Dabbous K.M., Reznik A.A, Mody B.J., Fulton F.P., Taber J.J. (1976). *Gas-Water Capillary Pressure in Coal at Various Overburden Pressure.* American Institute of Mining, Metallurgical, Petroleum inc.SPE 5348

Dallegge T. A. and Barker C. E. (2000). *Coal-Bed Methane Gas-In-Place Resource Estimates Using Sorption Isotherms and Burial History Reconstruction: An Example from the Ferron Sandstone Member of the Mancos Shale, Utah* - Chapter L of Geologic Assessment of Coal in the Colorado Plateau: Arizona, Colorado, New Mexico, and Utah. U.S. Geological Survey Professional Paper 1625–B, pp. L1–L26.

Dullien F.A.L (1991). *Porous Media Fluid Transport and Pore Structure*. Academic Press.

Donaldson.E.C.,Ewell. N and Singh.B.(1991).*Characteristics of Capillary Pressure Data*, *The Log Analyst*, Vol.29, No.1. pp 40-47.

Donaldson .C., Tiab D. (2004). *Petrophysics Theory and Practice of Measuring Reservoir Rock and Fluid Transport Properties.*

Firoozabady.A. Ramey.H.J. (1988). *Surface Tension of Water Hydrocarbon Systems at Reservoir Conditions.* Journal of Canadian Technology.Vol. 27,No.3.

Gale J., Freund P.(2001). *Coal-Bed Methane Enhancement with CO_2 Sequestration Worldwide Potential.* Environmental Geosciences. Vol.8, No.3, pp. 210-217.

Gash B. W. (1991). *Measurement of Rock Properties in Coal for Coalbed Methane Production*. 66th Annual Technical Conference and Exhibition, Paper 22909, Dallas, pp. 221-230.

Gentzis T., Goodarzi F., Cheung, F. K. and Laggoun-Défarge F. (2008). *Coalbed Methane Producibility from the Mannville Coals in Alberta, Canada: A Comparison of Two Areas*. International Journal of Coal Geology, Vol. 74, pp. 237–249.

Ghorbani D., Pilisi N., Vasanthrajan S.(2012). *CO_2 Sequestration in Deep Water Sediment:Optimization and Parametric Studies* .Carbon Management Technology Conference. CMTC 151396.

Green D.P.(2007). *Capillary Pressure Curves Determining by Direct Measurement of Saturation Using Magnetic Resonance Imaging*. Green imaging Technologies, Fredericton, NB, Canada, Canadian Well Logging Society.

GRI (Gas Research Institute). (1996). *A Guide to Coalbed Methane Reservoir Engineering.* GRI-94-0397, Chapter 4.

Ham Y.S.(2011). *Measurment and Simulation of Relative Permeability of coal to gas and water* Department of Chemical and Petrolum Engineering Calgary, Alberta.

Harpalani.S., Amadei,K., ranz,Scott., Smealli.E. Rotterdam.I. (1999).*Compressibility of Coal and its Impact on Gas Production from Coalbed Reservoirs.* Rock mechanics industry, SBN9 0 5809 052 3.

Harpalani S. and Schraufnagel R. A. (1990). *Shrinkage of Coal Matrix Release of Gas and Its Impact on Permeability of Coal*. Fuel, Vol.69, May, pp. 551-556.

Harpalani S. and Chen G. (1995). *Estimation of Changes in Fracture Porosity of Coal with Gas Emission*. Fuel Vol. 74, No. 10, pp. 1491-1498.

Hassler G.L and Brunner E. (1945). *Measurment of Capillary Pressure in Small Core samples*. Trans.AIME ,160,114.

Hoch O., (2005).*The Dry Coal Anomaly – The Horseshoe Canyon Formation of Alberta, Canada*. SPE Annual Technical Conference and Exhibition, Paper SPE 95872, Dallas USA, pp.14.

Honarpour M. and Mahmood S. M. (1988). *Relative Permeability Measurements: An Overview.*SPE 18565.

Hyman L. A., Brugler M. L., Daneshjou D. H. and Ohen H. A. (1992). *Advances in Laboratory Measurement Techniques of Relative Permeability and Capillary Pressure for Coal Seams*. Quarterly Review of Methane from Coal Seams Technology, pp. 9-16.

Issler. D.R.(1984). Calculation of Organic Maturation Levels for Offshore Eastern Canada—Implications for general Application of Lopatin's method. *Canadian Journal of Earth Sciences*, Vol. 21,No. 4, pp. 477-488.

Izgec O., Demiral B., Bertin H. and Akin S. (2005). *Experimental and Numerical Investigation of Carbon Sequestration in Saline Aquifers.* SPE 94697.

Johnson E. F., Bossler D. P. and Naumann V. O. (1959). *Calculation of Relative Permeability from Displacement Experiments.* Petroleum Transactions, AIME, Vol. 216, pp. 370-372.

Johnston.P., Santillo.D. (2002). *Carbon Capture and Sequestration: Potential Environmental Impacts.* IPCC Workshop on Carbon Dioxide Capture and Storage.

Jones A. F., Bell G. J., Taber J. J., and Schraufnagel R. A. (1988). *A Review of the Physical and Mechanical Properties of Coal with Implications for Coal- Bed Methane*

Well Completion and Production. Coalbed Methane, San Juan Basin, Rocky Mountain Association of Geologists, pp. 169–182.

Kailas.B.G.(2012). *Effect of CO_2 Flooding on the Wettability of Fontainebleau Sandstone.* Submitted for the Master of engineering at Dalhousie University.

Law D. H. S., Van der Meer, L. H. G. and Gunter W. D. (2002). *Numerical Simulator Comparison Study for Enhanced Coalbed Methane Recovery Processes, Part I: Pure Carbon Dioxide Injection*. SPE Gas Technology Symposium, Paper SPE 75669, Calgary Canada, 30 Apr–02 May, pp.14.

Lenormand R. (2006). *Conventional and Special Core Analysis: Theory Overview.* Version 14.

Manoj . B., Kunjomana A.G. Chandrasekharan and K.A. (2009). *Chemical Leaching of Low Rank Coal and its Characterization using SEM/EDAX and FTIR.* Journal of Minerals & Materials Characterization & Engineering, Vol. 8, No. 10, pp. 821-832.

Martel A.T., Gibling M.R., Nguyen.M. (2001). *Brines in Carboniferous Coalfield, Atlantic Canada*. Applies Geochemistry Vol.16, pp.35-55.

Mavor M. J. (2006). *Expert Opinion of Matthew J. Mavor Concerning Coalbed Methane Reservoir Behavior - Prepared for Alberta Energy and Utilities Board*. Proceeding No. 1457147, pp.25.

Mukhopadhyay P.K. , Goodarzi F., Crandlemire A.L., Gillis K.S., Macneil D.J., Smith.W.D., (1998),*Comparison of Coal Composition and Elemental Distribution in Selected Seams of the Sydney and Stellarton Basin, Nova Scotia, Eastern Canada*., International Journal of Coal Geology Vol. 37,pp. 113-141.

Naylor R.D., Calder J.H., Ryan, R.J.(1992). *Controls on Formation of Upper Carboniferous Coals in the Intermontane Stellarton and Cumberland Basins of Atlantic Canada*. Proceedings of the 1992 Canadian Coal and Coalbed methane Geoscience Forum, Parksville, British Columbia, pp. 365–397.

NRC.(2010). *Advancing the Science of Climate Change*. National Research Council. The National Academies Press, Washington, DC, USA.

Oren E., Bakke S. and Arntzen J. (1998) *Extending Predictive Capabilities to Network Models. the SPE Annual Technical Conference & Exhibition held in San Antonio, U.S.A., pp. 5-8.*

Paterson L., Meany K. and Smyth M. (1992). *Measurements of Relative Permeability, Absolute Permeability and Fracture Geometry in Coal*. Coalbed Methane Symposium, Townsville, Queensland Australia, pp. 79- 86.

Plug W.J., Mazumder S., Briuning J. (2008). Capillary Pressure and Wettability Behavior of CO_2 Sequestration in Coal at Elevated Pressures. SPE journal.

Price H. S. and Abdalla A. A. (1972). *A Mathematical Model Simulating Flow of Methane and Water in Coal*, US Bureau of Mines, Final Report.Vol.10, No.72, pp. 41.

Price J. and Smith B. (2008). *Geologic Storage of Carbon Dioxide Staying Safely Underground*. International Energy Agency (IEA).

Puri R., Evanoff J. C. and Brugler M. L. (1991). *Measurement of Coal Cleat Porosity and Relative Permeability Characteristics*. *SPE Gas Technology Symposium*, Paper 21491, Houston Texas, pp. 93–104.

Rapaka S. (2009*). Fluid Flow and Transport Phenomena During Geological Sequestration of Carbon Dioxide.*

Ritter.L.C. and Drake.R.L. (1945).*Pore Size Distribution in Porous Material*. Chemical Engineering Fundamentals.Vol. 17, pp. 782.

Robertson E. P. and Christiansen R. L. (2007). *Modeling Laboratory Permeability in Coal Using Sorption-Induced-Strain Data*. SPE Annual Conference and Exhibition, Paper 97068, Dallas, Texas, pp. 260–269.

Seidle. J. (2011). *Fundamentals of Coalbed Methane Reservoir Engineering.*

Stevens S. H. (1998). *Enhanced Coalbed Methane Recovery Using CO_2 Injection: Worldwide Resource and CO_2 Sequestration Potential.* SPE 48881; Denis Spector, Advanced Resources International, Inc. Pierce Riemer, IEA Greenhouse Gas R&D Program.

Taber J. J., Fulton P. F., Dabbous M. K. and Reznik A. A. (1974*). Development of Techniques and the Measurement of Relative Permeability and Capillary Pressure Relationships in Coal*. USBM Contract Final Report (Contract no. G0122006) .

Van Krevelen D. W. (1993). *Coal Typology-Physics-Chemistry-Constitution.* Third Edition, Elsevier Science Publishers, Amsterdam.

.
Wallington T. J., Srinivasan J., Nielsen O. J., Highwood E.J. (2004). *Greenhouse Gases and Global Warming Effect*. Environmental and Ecological Chemistry; EOLSS.

Wang G., Massarotto P. and Rudolph, V. (2004). *Studies of CBM Recovery and CO_2 Sequestration in Australia*. Proceedings of the 5th International Symposium on Mining Science and Technology, Xushou China,Vol. 20,No. 22, pp. 283-289.

Zhangxin C., (1962) .*Reservoir Simulation Mathematical Techniques in Oil Recovery*.

Appendix A: EDS and elemental analysis

C

Element	Weight%	Atomic%
C	83.80	87.91
O	14.39	11.33
Al	0.33	0.15
Si	0.39	0.17
S	1.09	0.43

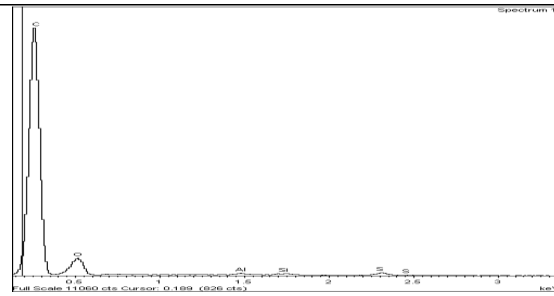

D

Element	Weight%	Atomic%
C	85.14	89.03
O	12.76	10.10
Al	0.71	0.33
Si	0.78	0.35
S	0.51	0.20

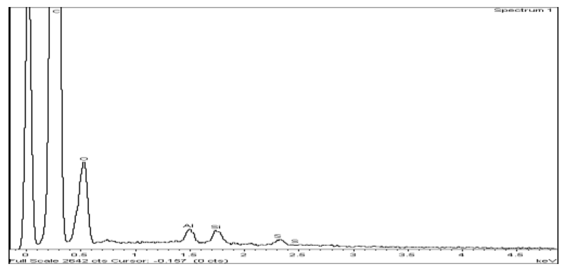

E

Element	Weight%	Atomic%
C	87.73	90.80
O	11.35	8.82
Al	0.16	0.07
Si	0.30	0.13
S	0.45	0.17

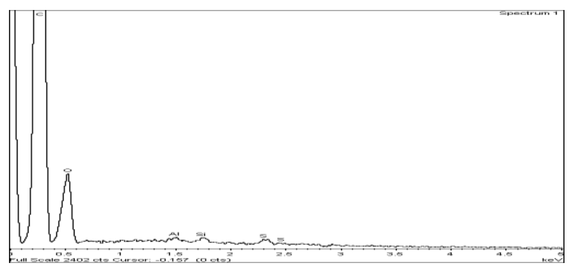

F

Element	Weight%	Atomic%
C	65.62	74.72
O	24.47	20.83
Al	2.66	1.34
Si	5.79	2.81
S	1.09	0.46
k	0.37	0.13

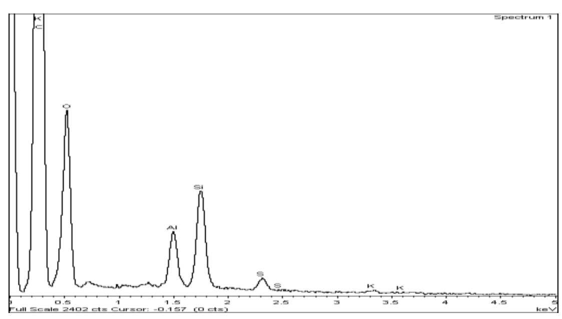

APPENDIX B: CAPILLARY PRESSURE DATA FOR THE SECOND RUN AT LABORATORY CONDITIONS FOR CO_2/BRINE SYSTEMS

Table B.1 Capillary Pressure Measurement of CO_2/Brine Systems For the Second Run

Pc	S_w	S_e	Log(S_e)	Log (P_c)
0.2	0.98	0.95	-0.02	0.70
1.3	0.95	0.89	-0.05	0.11
5.3	0.86	0.68	-0.17	0.72
10.3	0.67	0.25	-0.60	1.01
15.3	0.63	0.16	-0.79	1.18
21.3	0.59	0.07	-1.16	1.33
27.3	0.58	0.05	-1.34	1.44
31.3	0.56	0	-	1.49

To find saturation and capillary pressure at reservoir condition at first bulk volume and pore volume at reservoir condition was determined. From Equation 2.22:

$dV_B = 5\times 10^{-8} \times 85 \times (3280 - 14.7) = 0.013$

Bulk volume at reservoir condition is determined as:

$V_{B(res)} = V_{Bi} - dV_B = 85 - 0.013 = 84.987$

Therefore, pore volume at reservoir condition is determined from:

$V_{P(res)} = V_{B(res)} \times \varphi_{res} = 84.987 \times 0.056 \ = 4.76$

By having pore volume at reservoir condition and the volume of brine in the out flow, saturation data at reservoir condition is deduced.

With these data Figure B-1 is plotted:

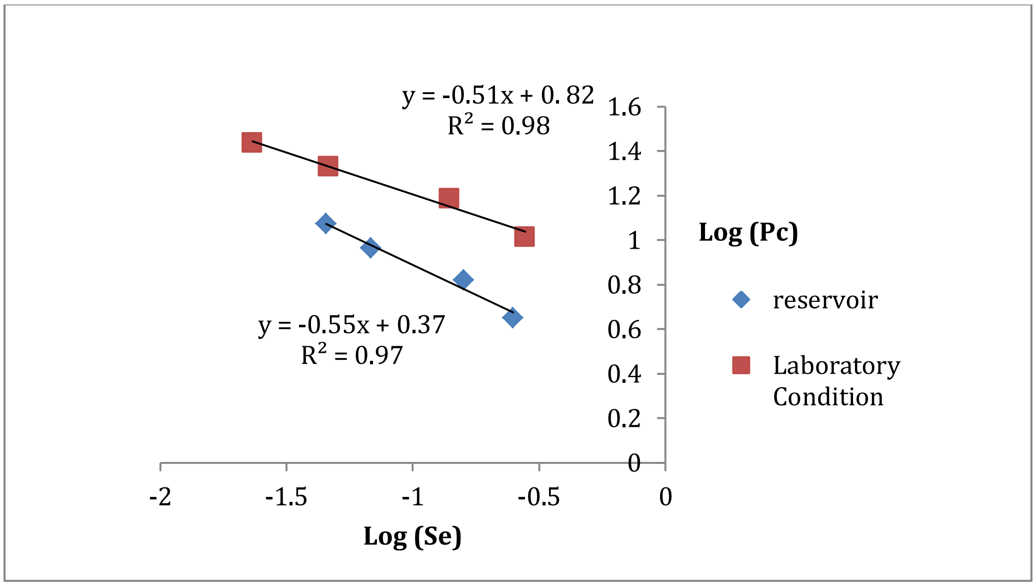

Figure B.1. Log-log plot of capillary pressure vs. effective saturation at laboratory and reservoir conditions (repeated experiment)

APPENDIX C: RELATIVE PERMEABILITY MEASUREMENTS FOR CO_2/ BRINE

Table C.1 Relative Permeability Determination for CO_2/ Brine

P_c	S_e	K_{rw}	K_{nrw}
0	0.95	0.813	0
0.2	0.89	0.625	0.002
1.3	0.68	0.211	0.054
5.3	0.25	0.004	0.526
10.3	0.16	0.001	0.686
15.3	0.07	0	0.860
21.3	0.05	0	0.900

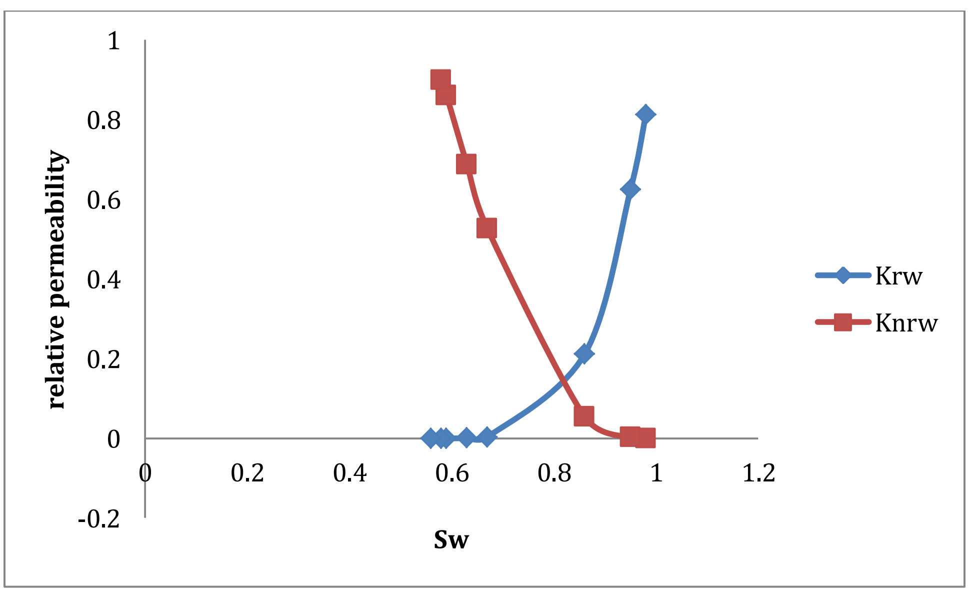

Figure C.1. Relative permeability for CO2/brine systems for the second run

APPENDIX D: TABLE OF LEAST SQUARES CALCULATION OF Y(P_C) AS A FUNCTION OF X(S_W)AND PORE SIZE DISTRIBUTION OF CO_2/ BRINE DRAINAGE FOR THE SECOND RUN

Table D.1 Pore Size Distribution Determination for the Second Run

y(P_c)	x(S_w)	x^2	xy	y^2	x^2y^2	r_i	D(r_i)
0.07	0.98	0.96	0.07	0.01	0.01	105.87	0
0.48	0.95	0.90	0.46	0.23	0.21	16.29	0.11
1.96	0.86	0.74	1.69	3.84	2.84	3.99	1.27
3.81	0.67	0.45	2.55	14.52	6.52	2.06	1.36
5.66	0.63	0.40	3.57	32.04	12.71	1.38	2.06
7.88	0.59	0.35	4.65	62.09	21.62	0.99	2.31
10.10	0.58	0.34	5.86	102.01	34.32	0.77	2.88
11.58	0.56	0.31	6.48	134.10	42.05	0.68	3.04

A,B and C were calculated as below:

NUM(1)= sum(X^2) ×[sum (XY) ×sum (XY^2)- sumY× sum ($X^2 \times Y^2$)] + sum XY) × [sumX× sum (X^2Y^2) – sum (XY) ×sum (X^2Y)]+sum (X^2Y) × [sumY×sum (X^2Y)-sum X×sum (XY^2)]

NUM(2)= [sum(X^2Y) ×sum(XY^2)-sum(XY) sum (X^2Y^2)]+sumX× [sumY×sum (X^2 Y^2) - sum(XY) ×sum(XY^2)+sum(XY) × [sum(XY) ×sum(XY) - sumY×sum(X^2Y)].

$NUM(3)=N\times (sum(X^2) \times sum(XY^2) - sum(XY) \times sum(X^2Y)]+sumX\times [sumY\times sum(X^2Y$
$-sumX \times sum(XY^2) + sum(XY) \times [sumX\times sum(XY) - sumY\times sum(X^2)]$

$DENOM= N\times [sum(X^2Y) \times sum(X^2Y) - sum(X^2)sum(X^2Y^2)] + sumX\times [sumX\times sum(X$
$^2Y^2)] - sum(XY) \times sum(X^2Y)] +[sum(XY) \times sum(X^2)-sumX\times sum(X^2Y)]$

A=NUM(1)/DENOM= -19.1

B=NUM(2)/DENOM= 9.56

C=NUM(3)/DENOM= - 10.2

Now by obtaining A, B and C, and substituting them in Eq. 2.24, ds/dp for each capillary pressure was determined as below:

$$\frac{dS_w}{dP_c} = -\frac{(1+CS)^2}{B+AC}$$

And then by having ds/dp. Surface area distribution ($D(r_i)$) was calculated by using below formula:

$$D(r_i) = \frac{P_c V_p}{r}\frac{dS_w}{dP_c}$$

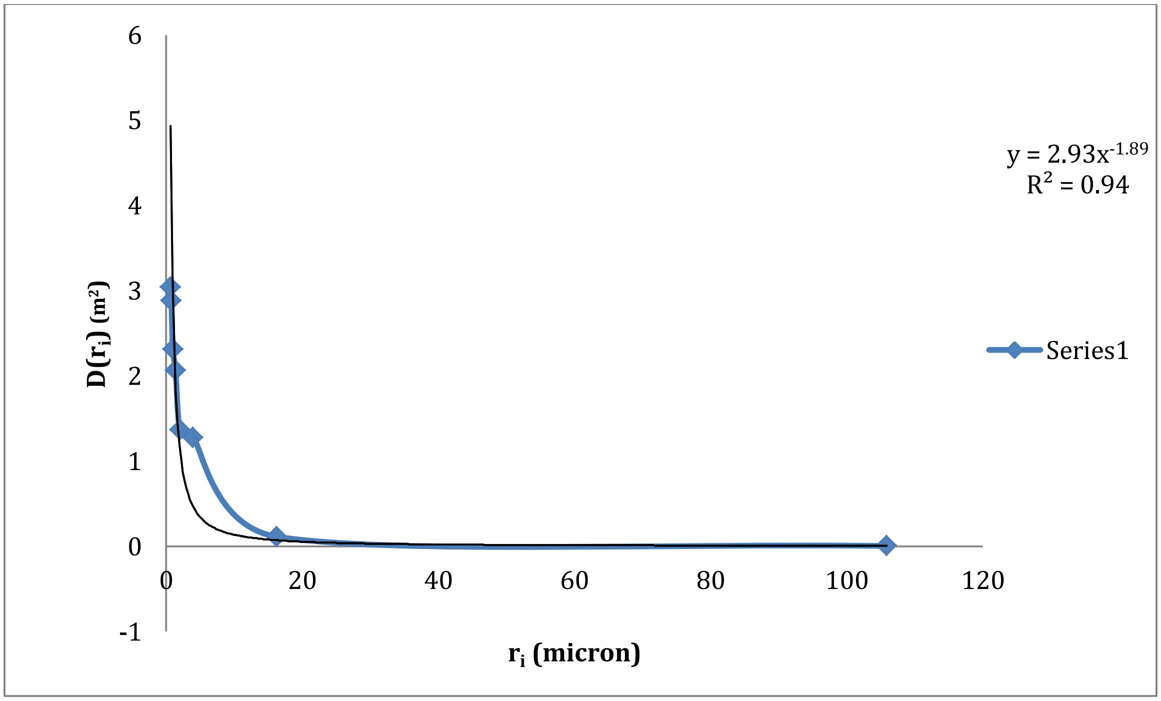

Figure D.1. Pore size distribution for CO_2 /brine for the second run

APPENDIX E: CAPILLARY PRESSURE DATA FOR THE SECOND RUN VERSUS SATURATION AT LABORATORYS

Table E.1 Capillary Pressure Measurements of Methane/Brine for the Second Time

P_c	S_w	S_e	$Log(S_e)$	$Log\ (P_c)$
0.2	0.98	0.94	-0.03	0.14
1.3	0.95	0.84	-0.074	0.95
5.3	0.89	0.66	-0.18	1.56
10.3	0.82	0.44	-0.36	1.85
15.3	0.74	0.19	-0.73	2.02
21.3	0.7	0.06	-1.20	2.17
27.3	0.68	0.00	-	2.27

Using these data, a graph of log-log capillary pressure versus saturation is plotted in Figure E-1 :

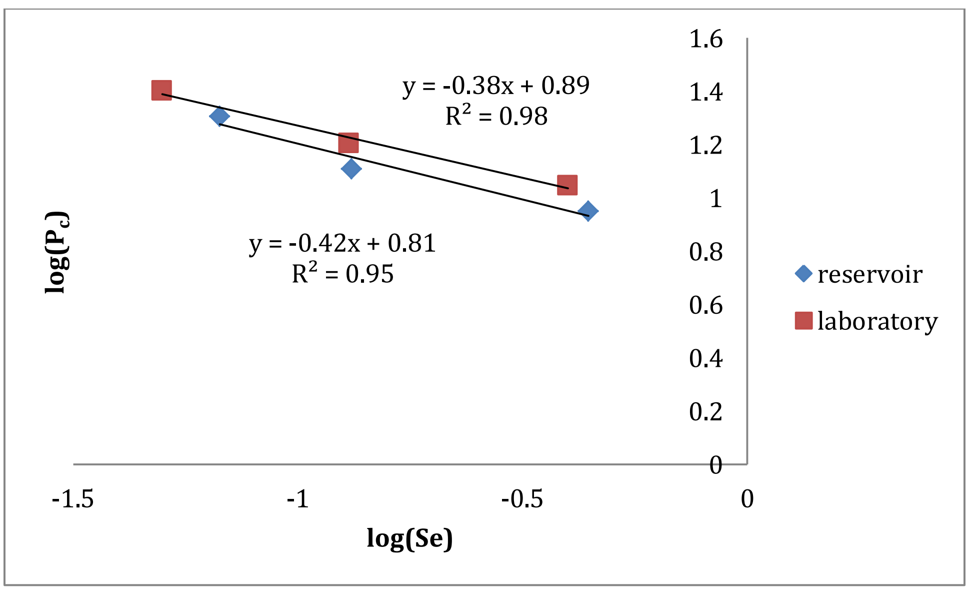

Figure E.1. Log-log plot of capillary pressure vs. effective saturation at reservoir conditions (repeated experiment)

APPENDIX F: RELATIVE PERMEABILITY MEASUREMENTS FOR METHANE/ BRINE SYSTEM

Table F.1 Relative Permeability Measurements of Methane/Brine

P_c	S_e	K_{rw}	K_{nrw}
0.2	0.94	0.809	0
1.3	0.84	0.510	0.008
5.3	0.66	0.223	0.071
10.3	0.44	0.051	0.266
15.3	0.19	0.001	0.642
21.3	0.06	0	0.88
27.3	0	0	1

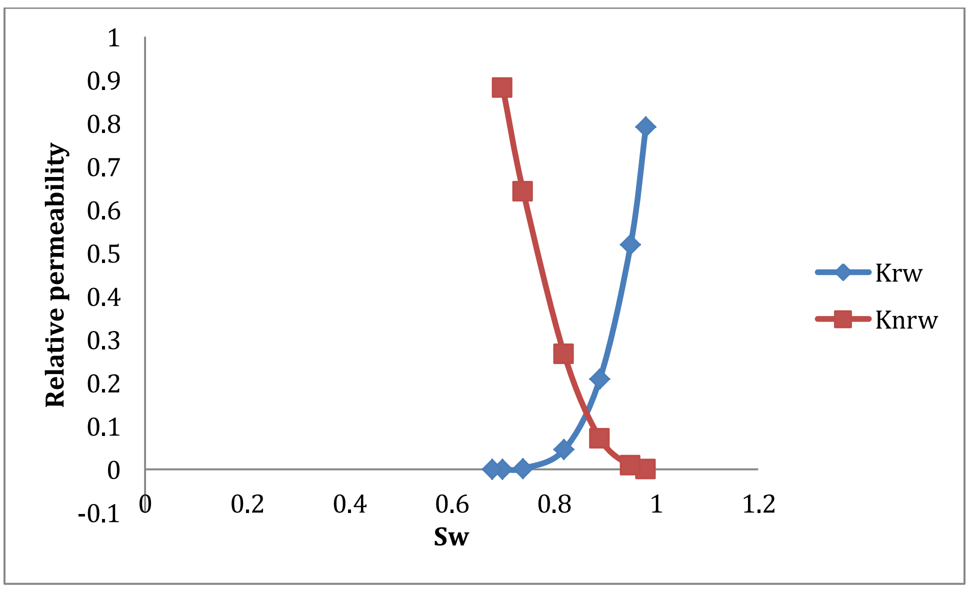

Figure F.1. Relative permeability measurement for methane/brine systems for the second run

APPENDIX G: LEAST SQUARES CALCULATION OF Y(P_C) AS A FUNCTION OF X(S_W) AND PORE SIZE DISTRIBUTION OF METHANE/ BRINE DRAINAGE FOR THE SECOND RUN

Table G.1 Data of Least Square Calculation for the Methane/Brine System

y(P_c)	x(S_w)	x^2	xy	y^2	x^2y^2	r_i	D(r_i)
0.3	0.98	0.96	0.29	0.09	0.09	105.87	0
1.4	0.95	0.90	1.33	1.96	1.77	17.29	0.002
4.5	0.89	0.79	4.01	20.25	16.04	3.89	0.037
9.1	0.82	0.67	7.46	82.81	55.68	2.06	0.237
13.1	0.74	0.55	9,69	171.61	93.97	1.38	0.866
21.2	0.7	0.49	14.84	449.44	220.23	0.89	1.989
24.8	0.68	0.46	16.86	615.04	284.39	0.76	3.542

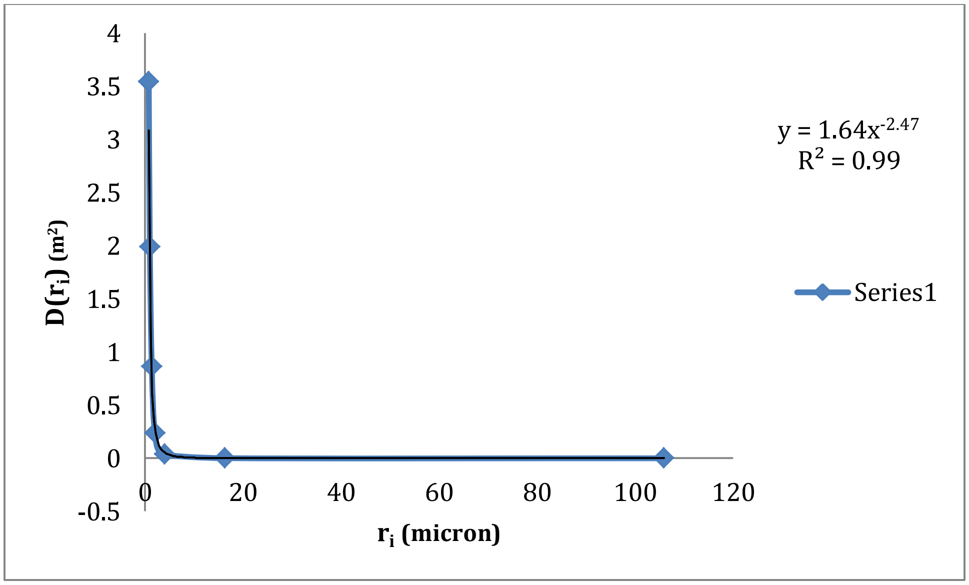

Figure G.1. Pore size distribution for methane/brine for the second run

APPENDIX H: BULK VOLUME, PORE VALUME AND CLEAT POROSITY MEASUREMENTS

Bulk volume measurements:

Bulk volume was calculated with direct measurement and Archimedes measurement through the following equations:

Direct measurement: $V_b = \pi\,(\frac{3.81}{2})^2\,7.59 = 86.48\ cm^3$

Archimedes measurement: $V_b = 486 - 400 = 85\ cm^3$

The results show that the core sample doesn't have the perfect cylindrical shape.

Error = 1.7 %

Pore volume measurements:

The initial dry core sample was weighed and found to be 111.7 g. Then the core sample was saturated with brine in vacuum oven for 48 hours. Then it was weighed and found to be 117.4 g. By placing these data in the Equation 3.1, the Pore volume was determined to be 5.58 cm^3.

Coal cleat porosity measurements:

Cleat Porosity of coal sample to brine can be determined by using gravimetric method. By substituting pore and bulk volume data into Equation3.2, Coal porosity to brine was found to be 0.065.

Cleat porosity at reservoir condition was determined as below:

$\Phi = 0.065\ [\exp\,(-4.5\times 10^{-5}\times(14.7-3280))] = 0.056$